MINISTERE DE L'ENSEIGNEMENT SUPERIEUR
ET DE LA RECHERCHE SCIENTIFIQUE
Felix Houphouet-Boigny university

UNITE DE FORMATION ET DE
RECHERCHE SCIENCES DES
STRUCTURES DE LA MATIERE ET DE
TECHNOLOGIE

RÉPUBLIQUE DE CÔTE D'IVOIRE
UNION - DISCIPLINE - TRAVAIL
Institute of Energy and Climate Research –
Fundamental Electrochemistry (IEK-9),
Forschungszentrum Jülich

Nº: 663

SPONSORED BY THE
Federal Ministry
of Education
and Research

MASTER
IN RENEWABLE ENERGY AND CLIMATE CHANGE

SPECIALITY: PRODUCTION AND TECHNOLOGY OF GREEN HYDROGEN

MASTER THESIS:

Subject/Topic:

INVESTIGATION OF MAIN CONTRIBUTORS IN SOLID OXIDE CELL (SOC) BY MULTIVARIATE REGRESSION

Presented on September 26, 2023 by:

Gbenga JEROME

JURY:

Prof. Obrou Kouadio Olivier	**President**	**Full Professor UFHB**
Dr Essy Kouadio Fodjo	**Examiner**	**Associate Professor UFHB**
Dr Koffi Aka Stephan,	**Major Supervisor**	**Associate Professor UFHB**
Prof. Dr. Rüdiger A. Eichel	**Co- Supervisor**	**Chair IEK-9/Full Professor RWTH**

ACADEMIC YEAR: 2022-2023

ACKNOWLEDGEMENTS

All gratitude goes to Almighty God for his inestimable love and grace He has endowed upon me throughout my undergraduate study and to carry out this project work.

I sincerely appreciate The Federal Ministry of Education and Research (BMBF) and the West African Science Service Centre on Climate Change and Adapted Land Uses (WASCAL) for providing this program's scholarship and financial support. Special thanks go to WASCAL Cote d'Ivoire and the University of Felix of Houphouet Boigny (UFHB) for hosting this program.

I would also like to extend my heartfelt appreciation to my major supervisor, Dr Koffi Aka Stephan (Associate Professor UFHB), whose insightful perspective and dedicated contribution have enriched the quality of my research work. His expertise and constructive feedback played a significant role in sapping the outcome of my research. I am deeply grateful to my co-supervisor, Prof. Dr. Rüdiger-A. Eichel (Chair IEK-9/Full Professor RWTH) for his unwavering support, profound expertise and invaluable guidance throughout my research period. His commitment to excellence has been a driving force behind the success of my research work. I would also like to thanks the jury members on there outstanding job during the defensed. The examiner Prof Essy Kouaolio Fodjo (Associate Professor UFHB) and the president Prof. Obrou Kouadio Olivier (Full Professor UFHB) who was very instrumental in handling the program

My sincere appreciation goes to my daily supervisor, Mänken Christian, who did more than supervision but drilled out the best in me. Your thorough scrutiny and constructive criticism made this work see the light of the day. I equally acknowledge Dr. Dominik Schafer and Dr. Felix Kunz's exceptional leadership, guidance and the excellent work atmosphere they have created during my research stay at IEK-9 Julich Forschunzentrum.

Lastly, I want to appreciate my family and friends, who are God's gift to me and with whom the journey and experience of this master's degree were worthwhile. Thank you all for your love and support. May you enjoy God's favour and mercy in every sphere of your life.

ABSTRACT

Durability and degradation-related issues affect the commercialisation of Solid Oxide Cell (SOC) technologies. Over the last decades, SOC technologies have been developed with significant progress in material development, understanding of degradation phenomena and performance-related issues. However, individual operating parameters' influence on the overall SOC degradation is still not fully understood. This thesis aims to investigate the main contributors to SOC degradation using multivariate regression analysis. Different load operations from stack experiments with homogenous properties were collected, and the degradation rate for each load operation with their corresponding operating conditions, such as current density, conversion rate and stack temperature, were determined. After consolidation of the dataset, a multivariate regression analysis was used to examine each contributor's relevance to SOC degradation. To quantify the level of uncertainty, a Bayesian multivariate regression model using PyMC3 was employed. This analysis reveals that operating current density is the main contributor to SOC degradation. The influence of conversion rate, however, cannot be neglected as the conversion rate is the second leading contributing factor to SOC degradation.

Keywords: SOC, operating conditions, current density, stack temperature, conversion rate, Bayesian Analysis, Multivariate Regression, PyMC3

RÉSUMÉ

Les problèmes liés à la durabilité et à la dégradation affectent la commercialisation des technologies de cellules à oxyde solide (COS). Au cours des dernières décennies, les technologies COS ont été développées avec des progrès significatifs dans le développement des matériaux, la compréhension des phénomènes de dégradation et les problèmes liés aux performances. Cependant, l'influence des paramètres de fonctionnement individuels sur la dégradation globale du COS n'est pas encore entièrement comprise. Cet project de recherche vise à étudier les principaux contributeurs à la dégradation du COS à l'aide d'une analyse de régression multivariée. Différentes opérations de chargement issues d'expériences de pile présentant des propriétés homogènes ont été collectées et le taux de dégradation pour chaque opération de charge avec les conditions de fonctionnement correspondantes, telles que la densité de courant, le taux de conversion et la température de la pile, ont été déterminés. Après consolidation de l'ensemble de données, une analyse de régression multivariée a été utilisée pour examiner la pertinence de chaque contributeur dans la dégradation du COS. Pour quantifier le niveau d'incertitude, un modèle de régression bayésien multivarié utilisant PyMC3 a été utilisé. Cette analyse révèle que la densité de courant de fonctionnement est le principal contributeur à la dégradation du COS. L'influence du taux de conversion ne peut cependant pas être négligée, car le taux de conversion est le deuxième facteur contribuant à la dégradation du COS.

Mot clé : SOC, conditions opératoires, densité de courant, température de cheminée, taux de conversion, Analyse Bayésienne, Régression multivariée, PyMC3

ABBREVIATION AND NOMENCLATURE

ABBREVIATION	DESCRIPTION
SOC:	Solid Oxide Cell
SOFC:	Solid Oxide Fuel Cell
SOEC:	Solid Oxide Electrolysis Cell
rSOC:	Reversible Solid Oxide Cell
ASR:	Area Specific Resistance
CTE:	Coefficient of Thermal Expansion
YSZ:	Yttria Stabilized Zirconia
ScSZ:	Scandia Stabilised Zirconia
LSGM:	Strontium Magnesium-Doped Lanthanum Gallate:
GDC:	Gadolinia-Doped Ceria
CGO:	Cerium Gadolinium Oxide
HOR:	Hydrogen Oxidation Reaction
ORR:	Oxygen Reduction Reaction
OER:	Oxygen Evolution Reaction
MIEC:	Mixed Ionic and Electronic Conductors
LSM:	Lanthanum Strontium Manganite
TPB:	Triple Phase Boundary
LSC:	Lanthanum Strontium Cobaltite
LSCF:	Lanthanum Strontium Cobalt Ferrite
MCF:	Manganese Cobalt Ferrite
HDI:	Highest Density Interval
r_hat:	Potential Scale Reduction Factor

NOMENCLATURE	DESCRIPTION
ΔG	Change in Gibbs's Free Energy ($Jmol^{-1}$)
ΔH	Change in Enthalpy ($Jmol^{-1}$)
ΔS	Change in Entropy (J/K)
$\Delta G°$	Standard Gibb's Free Energy Change ($Jmol^{-1}$)
$E°$	Ideal Standard Potential (V)
W_{el}	Electrical Work (J)
E_{rev}	Reversible Cell Potential (V)
E_H	Thermoneutral Voltage (V)
E_N	Nernst Potential (V)
η_{act}	Activation Loss (V)
η_{ohm}	Ohmic Losses (V)
j	Current Density (A/cm^2)
$U_{cell\ i}$	Cell Voltage i (V)
T_{stack}	Stack Temperature (°C)
R	Universal Gas Constant ($Jmol^{-1}K^{-1}$)
F	Faraday Constant (C/mol)
D	Number of Predictors
n	Number of Electron Transfer
τ	Global Shrinkage Parameters
λ	Local Shrinkage Parameters
β_i	Regression Model Parameters

LIST OF FIGURES

TABLE OF CONTENTS

GENERAL INTRODUCTION

GENERAL INTRODUCTION

Human society's existence and expansion are linked to resource availability and utilisation. In meeting the ever-increasing needs of the world's growing population, such as power generation, heating, transportation, agriculture, and the advancement in civilisation, fossil fuel remains a significant energy resource in attending to this need. However, the combustion of fossil fuels results in the release of substantial amounts of greenhouse gases and emissions, exacerbating global warming and climate change and posing significant threats to human well-being ([1], [2]). The finite nature of fossil fuels and the imperative to curb greenhouse gas emissions responsible for global warming have become paramount concerns of the 21st century. In response, the international community has set an ambitious goal of achieving carbon neutrality by 2050. This goal reflects the urgent need to transition to sustainable energy sources and reduce our reliance on finite fossil fuels to mitigate the impact of climate change and secure a sustainable future for future generations. In pursuit of this goal, various incentives such as tax credits, carbon pricing, and emission reduction initiatives have been devised to promote the widespread adoption of renewable energy sources [3]. While there has been notable progress in increasing the share of renewable energy resources specifically for power generation, it remains insufficient to meet our needs. Renewable energy resources cannot be wholly used due to their intermittent nature, resulting in an imbalance between energy supply and demand [4]. To overcome this limitation, the development of new technologies for energy storage and conversion is essential. These technologies play a crucial role in addressing the temporary mismatch between energy demand and supply, ensuring a reliable and consistent energy transition [3].

Several energy storage and conversion technologies, such as pump hydro systems, thermal energy storage, flywheels, and batteries, are already in their mature stages [3]. However, these technologies are not suitable for every situation. Due to higher energy storage capacity for the same volume than batteries, hydrogen and other chemicals have gained increasing attention as potential storage mediums. Consequently, the focus on energy storage has shifted towards technologies employing fuel cells and electrolysers ([3], [5]). Reversible electrochemical cells offer a novel alternative, specifically Power to Gas and Gas to Power System. In instances of surplus electricity, the excess energy can be stored as chemical energy, primarily in the form of hydrogen, through the process of electrolysis. This stored chemical energy can then be converted into electricity through fuel cell operation. The capability of solid oxide cell to combine these operations within a single bifunctional unit make them attractive for energy

storage and generation [6]. Solid oxide technology has garnered significant attention from researchers because it can potentially play a crucial role in achieving decarbonisation and climate neutrality.

Initially, research focused primarily on investigating solid oxide cells in fuel cell mode. However, a reversible mode of operation has emerged as a promising option, enabling the combination of chemical energy storage and power generation. This advancement has expanded the potential usage times beyond relying solely on a single mode of operation ([3], [7]). Solid oxide cells can be operated in fuel cell mode as solid oxide fuel cells (SOFC), where they electricity from hydrogen and other energy resources such as hydrocarbon and carbon monoxide, or they can be operated in electrolysis mode as Solid oxide electrolysis cell (SOEC), where they produce hydrogen from H_2O when electricity is supplied. When operated in both SOFC and SOEC reversibly, it is termed reversibly Solid oxide cells (rSOCs) [8]. Solid oxide is a promising technology with more tremendous advantages than other energy storage and conversion devices; although operating at high temperatures, they consume less electricity, thus making them efficient in SOEC mode[9]. In SOFC mode, SOC features the highest efficiency and fuel flexibility when compared with other fuel devices. Moreover, SOC offers the opportunity to employ a single unit to generate electricity, heat and valuable fuels[7].

Reversible solid oxide cell offers a distinct possibility to produce electricity, heat and valuable fuels in a highly efficient system compared with other existing technology [48]. Despite the flexibility and excellent suitability for real-world application of SOC, which includes both SOFC and SOEC, several degradation-related challenges must be overcome to accelerate their commercialisation and use in the present and future energy systems[29]. The ageing of the cell is one of the main problems with rSOC. When operating in fuel cell mode, fuel contaminants or impurities cause fuel electrode degradation. Ni-spreading and Ni-loss are the main causes of fuel electrode degradation when operating in electrolysis. The primary causes of oxygen electrode performance degradation are secondary phase development, Chromium poisoning through interaction with steel interconnect, and delamination of the oxygen electrode/electrolyte interface layer. The main degradation mechanisms identified in the electrolyte component of rSOC are phase transition, mechanical failure and dopant diffusion [29]. In addition to material-related problems, specific operating conditions such as temperature, current density, fuel utilisation, and steam utilisation can cause the degradation of SOC in the long term [48].

Although processing and material engineering improvements have significantly improved SOC performance, the impact of different operating conditions is still not fully understood. This thesis aims to quantitatively and qualitatively analyse the relevance of individual contributors to SOC stack degradation via regularised multivariate regression with data from long-term experiments. Long-term experimental data from Forschungzentrum Julich is used for this analysis. Forschungzentrum Julich is a renowned research centre actively researching solid oxide cells and their testing. It has contributed significantly to the development and understanding of this technology. As one of the focus areas at the Institute of Climate and Energy (IEK-9), the centre has conducted extensive experimental studies to investigate the durability, performance and degradation of SOCs under various operating conditions. With the availability of these experimental stack data with similar properties, the operating conditions contributing to SOC degradation can be investigated. The following objectives will have to be achieved during the thesis:

- Investigation and identification of different load phases suitable for evaluation in long-term stack experiments;
- Labelling of phases within individual operating conditions and prior occurrence of operational incidents;
- Derivation of degradation measurement for each load phase;
- Application of regularised multivariate regression to identify the main contributor to SOC stack degradation with PyMC3 framework;
- Determination of the most influential operating parameters and events based on the determined phase and multivariate regression analysis.

CHAPTER I:

LITERATURE REVIEW

CHAPTER I: LITERATURE REVIEW

Introduction

This chapter presents a comprehensive review of existing scholarly work concerning SOC degradation in the context of the influence of operation conditions on SOC degradation. It delves further into the working principle and thermodynamics of SOC operation, SOC material and configuration and the various degradation SOC degradation mechanism that has been proposed.

1 Review of Relevant Literature

Several factors can cause SOC stack degradation within the range of operating conditions, such as coarsening of catalytic particles, active site contamination by impurities, deposition of carbon and electrode delamination, causing the degradation of the electrochemical performance of SOC. Most degradation phenomena have effects closely related to fuel used, composition and impurities contained, and the set of operating conditions, including operating temperature, the degree of reactant utilisation, and operating current densities ([7], [10]). Therefore, identifying and quantifying diverse degradation processes at different levels is required to select optimal operation conditions.

Hagen et al. [11] investigate anode-supported solid oxide cell's degradation behaviour as a function of operating temperature current density. This study's test matrix comprised temperatures 950°C, 850°C and 750°C and current densities between 0.2 A/cm^2 and 1.9A/cm^2. The study reveals that the degradation rate increases with increasing current density, which is more pronounced even at lower temperatures. Conversely, a lower degradation rate was observed at higher temperatures, even at high current density. Further post-test analysis shows that degradation of the cathode was the dominant contributor to cell degradation at high current densities and low temperatures, while the anode was found to contribute more at higher temperatures.

The performance of solid oxide fuel cells under severe operating conditions was studied by Koch et al. [12]. Anode-supported cells with a double-layer LSM cathode were operated at 750°C or 850°C with hydrogen with 5% or 50% water at current densities ranging from 0.25Acm^{-2} to 1Acm^{-2} in order to study the effect of humidity on SOC degradation. These cells had resistance corrected for fuel utilisation to ensure they were quite similar. They were subjected to varying operating conditions. The study reveals that the degradation rates were

generally higher at high current densities than at lower current densities. In addition, for some temperatures and current densities, a high water content results in a higher degradation rate. The testing conditions to which the cells were subjected reveal a critical cell voltage below which fast degradation is observed.

EU integrated Project "Real SOFC" is a study done to improve the understanding of degradation in SOFC stacks to extend the durability of SOFC stacks. A series of stacks comprising two or four planar anode-supported cells were operated for 3000h to 1000h to better understand the degradation of SOFC stacks as a function of operation conditions while the choice of fuel, varying fuel utilisation and current density was investigated. The study revealed that the choice of fuel does not influence the degradation behaviour of the short stacks and is hardly influenced by fuel utilisation in the range of 8-75%[13].

After operating a four-layer anode-supported solid oxide fuel cell stack with hydrogen fuel of up to $1Acm^{-2}$ and a fuel utilisation rate of 80% for more than 10,000 hours, Fang et al.[14], observed that the degradation rate varied with different operating parameters, increasing with current density and fuel utilisation rate. However, a clear tendency in the current density or fuel utilisation cannot be concluded. The study further reveals that higher fuel utilisation may impact the degradation behaviour more than the current density.

Yang et al. [15] investigated the effect of operating conditions on the performance degradation of anode-supported Ni-YSZ single solid oxide fuel cells with $0.5Acm^{-2}$ active area. This study subjected eight cells to different operating temperatures and current densities to examine the performance degradation. All the cells experience rapid degradation at the initial state under different current densities, and high current density promotes degradation at the initial stage. The duration of rapid initial degradation was shortened as temperatures increased from 700°C-800°C. The study further revealed that at the same temperature, operating the cell at higher current densities leads to higher degradation; while operating at the same current densities, the degradation rate decreases when temperatures increase.

Apart from this study, quantifying the impact of individual operating conditions on the degradation of solid oxide cells has not yet been investigated.

2 Theoretical Background

2.1 Structure of Solid Oxide Cell

Solid oxide cell is a class of electrochemical devices capable of converting chemical energy into electrical and vice versa by promoting a redox reaction, reduction, and simultaneous oxidation of reactants across an ionic conductive membrane at a high temperature ([16], [17]). SOCs are high-temperature, all-solid devices with two distinct functions: solid oxide electrolysis cells (SOECs), which store renewable electric energy from solar panels and wind turbines in hydrogen fuel, and solid oxide fuel cells (SOFCs), which convert the chemical energy of fuels like hydrogen, natural gas, and other hydrocarbons to electricity [18].

In principle, the basic components of SOC are fuel or hydrogen electrodes, electrolytes and air or oxygen electrodes. When a Solid Oxide cell operates in fuel mode (SOFC), gaseous fuel such as H_2 is oxidised into H^+ ions at the fuel or hydrogen electrode, releasing two electrons. At the oxygen electrode, O_2 is adsorbed and reduced to O^{2-} by taking electrons released from the hydrogen electrode transported through an external circuit. As a result of the oxygen partial pressure difference between the hydrogen electrode and oxygen electrode, the O^{2-} moves through the oxide conducting electrolyte and reacts with H^+ to H_2O at the hydrogen electrode, as shown in Figure 1A. The reaction that occurs at the fuel electrode and air electrode during SOFC mode are as follows:

H_2 Oxidation at the fuel electrode:

$$H_2 + O^{2-} \rightarrow H_2O + 2e^- \qquad \text{I.1}$$

O_2 reduction at the air electrode

$$\frac{1}{2}O_2 + 2e^- \rightarrow O^{2-} \qquad \text{I.2}$$

Overall reaction

$$H_2 + \frac{1}{2}O_2 \rightarrow H_2O \quad \Delta H^o = -241.8 kJ/mole \qquad \text{I.3}$$

When operating in fuel cell mode, SOFCs offer a reliable substitute for traditional combustion technology in producing electrical power. One of SOFCs' primary benefits is its exceptional fuel versatility, which includes hydrogen, methanol, ethanol, natural gas, and hydrocarbons. Additionally, they are suited for stationary applications with great scalability and dispersed power supply ([19], [20]).

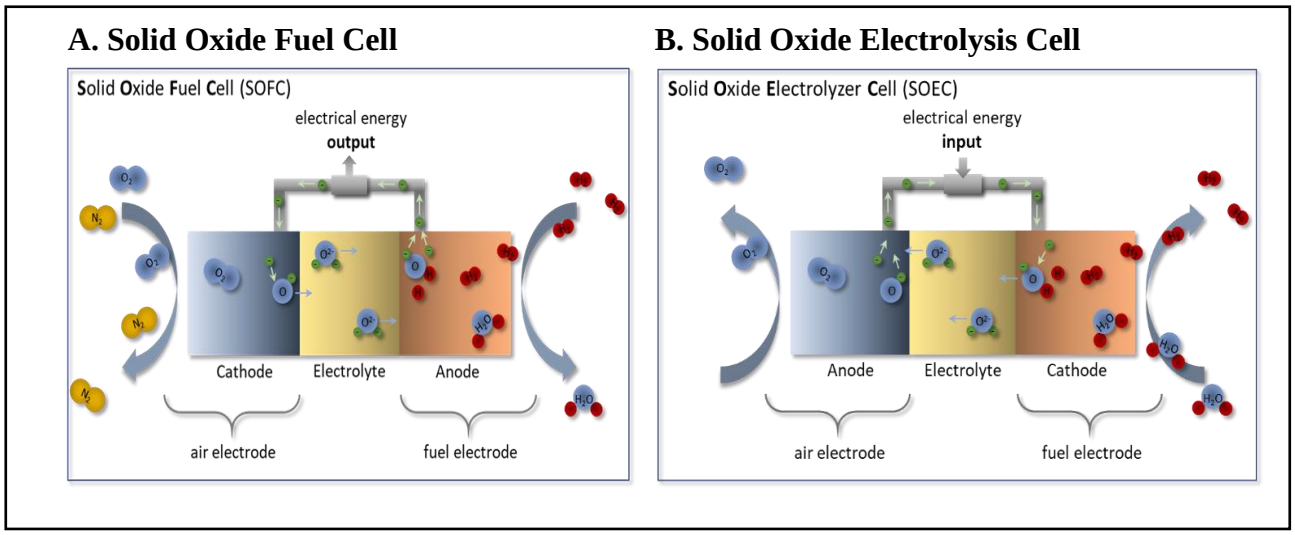

Figure 1: *Working Principle of SOFC and SOEC* [21]

In the SOEC operating mode, heat and electrons are supplied by external power sources at the hydrogen or fuel electrode side, where they are electrochemically split into H_2O and oxygen ions. The oxygen ion diffuses through the electrolyte, releasing O_2 when reaching the oxygen electrode, releasing two electrons ([22], [23]). The working principle of SOEC is depicted in Figure 1B. The reaction during SOEC occurs in SOEC mode as follows:

Reduction at the fuel electrode:

$$H_2O + 2e^- \rightarrow H_2 + O^{2-} \qquad \text{I.4}$$

Oxidation at the Air electrode:

$$O^{2-} \rightarrow \frac{1}{2}O_2 + 2e^- \qquad \text{I.5}$$

Overall Reaction

$$H_2O \rightarrow H_2 + \frac{1}{2}O_2 \quad \Delta H^o = +241.8 kJ/mole \qquad \text{I.6}$$

Unmatched conversion efficiencies result from favourable thermodynamics and kinetics at higher working temperatures, making SOEC technology attractive. Steam (H_2O), carbon dioxide (CO_2), or both can be directly electrochemically converted into hydrogen (H_2), carbon monoxide (CO), or syngas (H_2+CO), respectively, using SOECs. The co-electrolysis of CO_2 and H_2O using SOEC technology is a promising means of hydrocarbon fuel production while recycling greenhouse gas emissions ([22], [24]).

2.2 Thermodynamics of rSOC

The theoretical work that can be obtained by oxidising a mole of fuel can be expressed as:

$$\Delta G = \Delta H - T\Delta S \quad \text{I.7}$$

Where ΔH is enthalpy change, which represents the total thermal energy available. ΔS is the entropy change. The term $T\Delta S$ in the equation represents the unavailable energy resulting from the change in entropy within the system. Depending on the choice of fuel used, a fuel cell reaction with negative entropy generates heat, such as hydrogen oxidation, while those with positive entropy change extract heat from the surroundings if the reversible generation of heat is smaller than the reversible absorption of heat [25].

Considering an rSOC during fuel cell operation undergoing a reversible process under isothermal and isobaric conditions during which the reaction in equation I.3 occurs. The change in the Gibbs free energy (G) equals the maximum electrical work by the system (W_{el}) obtained from the SOFC [26].

$$W_{el} = -\Delta G \quad \text{I.8}$$

Electrical work is, in general, described by the relation:

$$W = EI\Delta t \quad \text{I.9}$$

Where E is the cell voltage, and I is the current. In a fuel cell reaction, electrons are transferred from the anode to the cathode, generating a current. The amount of electricity ($I\Delta t$)transferred when the reaction occurs is given by nF, where n is the number of electrons transferred, and F is Faraday's constant= 96,493 coulombs. The electrical work can hence be calculated as:

$$W_{el} = \Delta G = -nFE \quad \text{I.10}$$

Hence, the maximum cell potential or the reversible cell potential becomes:

$$E_{rev} = -\frac{\Delta G}{nF} \quad \text{I.11}$$

It is called reversible voltage because it is the maximum possible voltage without any irreversible losses. If all the potential chemical energy for a reaction went into electrical work without heat transfer, there would be no entropy change; $\Delta G = \Delta H$. In this case

$$E_H = \frac{-\Delta H^{\circ}}{nF} \quad \text{I.12}$$

$E_H\ is$ the thermoneutral voltage, which represents a theoretical upper limit and is essential to evaluate the entropy-related losses, especially in fuel cell operation. However, thermoneutral voltage is very important for the operation behaviour in electrolysis operation [27].

It is worth noting that the state function in equation I.7 is pressure and temperature-dependent. Since SOC operates at higher temperatures than the standard conditions, these voltages' temperature and pressure dependence should be considered. Kirchhoff's law can be used to account for variation due to temperature changes [27].

For a general equation or process of A and B, giving products C and D:

$$\alpha A + \beta B \ \rightarrow \gamma C + \delta D \qquad \text{I.13}$$

The Gibbs free energy can be expressed as:

$$\Delta G = \Delta G^o + RTln\frac{[C]^\gamma[D]^\delta}{[A]^\alpha[B]^\beta} \qquad \text{I.14}$$

Where each [A], [B], [C], [D] the thermodynamic activity coefficient for the reacting species and ΔG^o is the standard Gibbs free energy of the reaction at standard state. By dividing equation I.14 by nF, we obtain:

$$E_N = E^0 - \frac{RT}{zF}ln\frac{[C]^\gamma[D]^\delta}{[A]^\alpha[B]^\beta} \qquad \text{I.15}$$

Equation I.15 is the Nernst equation, which considers the reactant's activities and deviation from standard conditions. In general, the Nernst voltage provides a relationship between the ideal standard potential for the cell reaction and the cell voltage E at different concentrations of the reactants and products. This potential sets the upper limit or maximum performance achievable by a fuel cell. It provides a relationship between the ideal standard potential (E^0) for the cell reaction and the ideal equilibrium potential (E) at other partial pressures of reactants and products [25].

The actual cell potential is decreased from its ideal potential because of several irreversible losses. Figure 2 provides a qualitative description of the various loss mechanisms in fuel cell operation. The relative significance of each type of loss depends on the load applied. The graph in Figure 2 plots the cell voltage as a function of current density and is labelled with the contributions of the first three sources of loss described below.

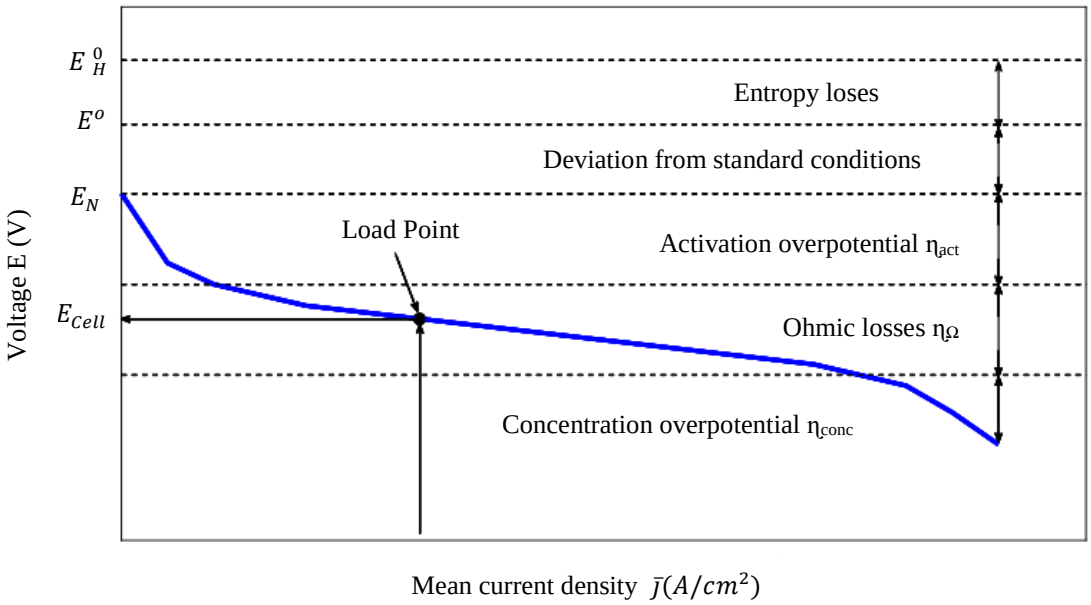

Figure 2: *SOFC Polarization Curve with the related loss* [27]

2.2.1 Activation Overpotential

Electrochemical and chemical reactions are quite similar in requiring the interacting species to overcome activation energy [25]. Activation losses can be considered as the potential to drive the reaction forward at the required rate at both electrodes. These losses stem from sluggish electrode kinetics and depend on the type of reaction, the electrocatalyst, electrode material and microstructure, and reactant reactivity. Activation losses can be calculated using equation I.16

$$\eta_{act} = \frac{RT}{\alpha nF} ln \frac{i}{i_o} \quad \text{I.16}$$

2.2.2 Ohmic losses

These are caused by the cell's resistance flow of ion ions in the electrolytes and electric current flow in the electrode. The electrolyte and fuel electrode obey Ohm's law. Therefore, ohmic losses can be expressed by equation I.17

$$\eta = iR \quad \text{I.17}$$

i is the current density, and R is equivalent to the total cell resistance, which includes electronic, ionic and contact resistance [25]. The main contributor to this overpotential is typically ionic transport rather than electronic transfer. However, it is necessary to consider the intrinsic conductivities of the different materials, the cell and stack shape, and the convolution of the

conduction routes in the porous electrodes [17]. Area Specific Resistance (ASR) is the ohmic resistance normalised by the active cell area. ASR is an important performance parameter in rSOC, where the ohmic losses often dominate the overall polarisation of the cell [28].

2.2.3 Concentration Overpotential

These are caused by the reactants' finite mass transport constraints and are highly dependent on the current density, reactant activity, and electrode structure. When finite mass transport rates restrict the supply of fresh reactant and the evacuation of products, the products frequently dilute a reactant consumed at the electrode by an electrochemical reaction. As a result, a concentration gradient develops, driving the mass transport procedure. Gas diffusion mechanisms regulate mass transfer in a fuel cell that only uses gaseous reactants and products (such as SOFC)

Solid Oxide Electrolysis Cells (SOEC) behaviour is similar to SOFCs. Therefore, the thermodynamic principle described during SOFC applies to SOEC but in the reversed mode. In electrolysis operation, the total energy required to split water into hydrogen and oxygen is the opposite of enthalpy of formation as seen in equation I.6

Due to the positive enthalpy and the positive Gibbs free energy of the reaction, the reaction is not spontaneous; hence, energy input is required to drive the process. $\Delta G = W_{elec}$corresponds to the electrical energy and $T\Delta S$ heat energy needed for electrolysis. The electrolysis cell can be operated below or above the thermoneutral voltage, leading to endothermic or exothermic operation. The so-called thermoneutral operating point is attained when the cell voltage and thermoneutral voltage match. The ability to introduce the entropy term as heat in endothermic operation makes obtaining extremely high electric efficiency possible. Against this background, an endothermic and particularly thermoneutral operation is preferable. The relationship described concerning the various loss mechanisms remains valid for electrolysis operation [27]. Figure 3 shows the voltage-current density curves for SOEC.

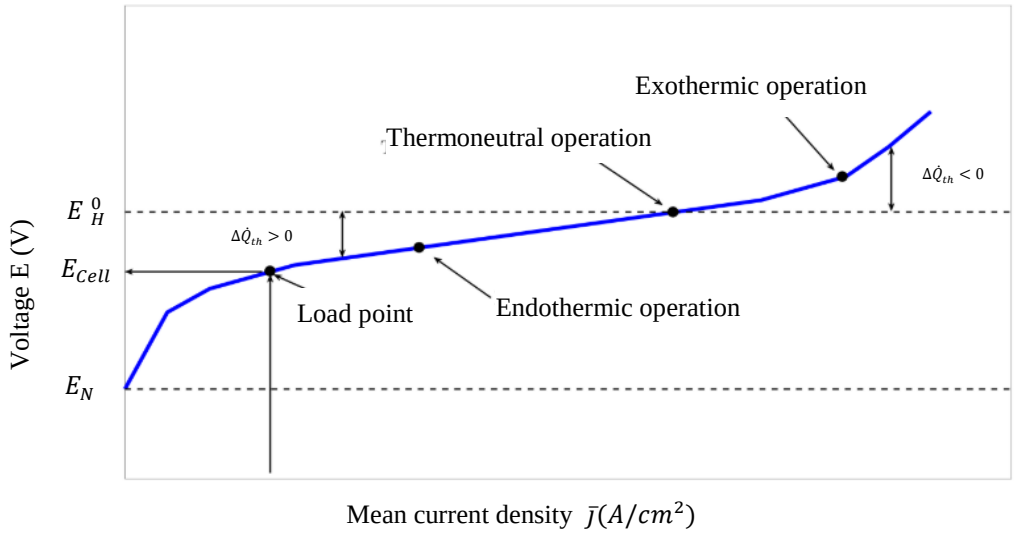

Figure 3: *SOEC Polarization Curve* [27]

3 Materials And Design Configuration

3.1 Design Configuration of rSOC

Two porous electrodes—an anode and a cathode—separated by a dense electrolyte make up the electrochemically active parts of traditional rSOC. To make the system work properly, each of these parts needs to have particular qualities. For instance, the anode and cathode's material composition and porous microstructure significantly impact their performance. Additionally, the electrolytes must be a good conductor of ions but not electrons [17]. For most practical applications, planar and tubular designs are the most common cell geometric for rSOC[29]. Figure 4 shows the schematic of the different SOC configurations.

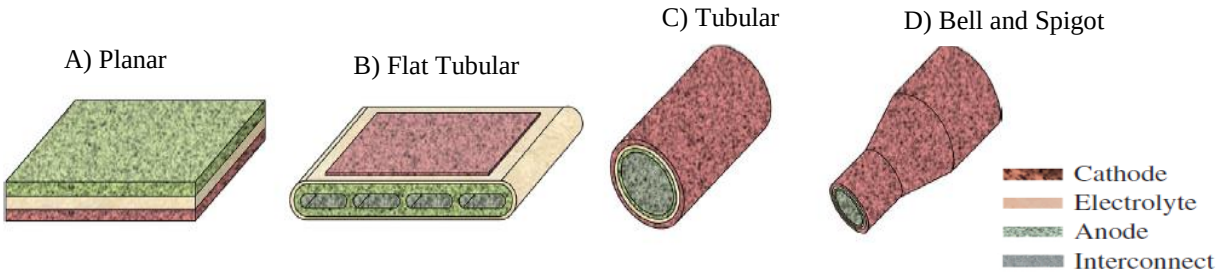

Figure 4: *SOC Design Configuration* [17]

The tubular cell comprises an array of sandwiched electrolytes and electrodes in a specific length and diameter. Early fuel cells were predominantly tubular in design, in part because these systems were much easier to seal, and tubular cell presents a more solid thermo-cycling performance, and some developers continue to pursue this design ([17], [29]). On the other hand, the planar design (radial or flat plate) includes a compact assembly of electrolytes and electrodes (Figure 5). Most commercially available systems today are in the planar configuration due to manufacturing considerations, optimal volumetric power density, and the ease of cell stacking [30]. The planar design has a simpler and cheaper fabrication procedure, higher power density, and low internal resistance due to its short current path. Both cell designs require sufficient mechanical strength to withstand the operation stresses provided by the support layer. The support layer has the largest thickness, and the thickness of other layers is minimised to avoid high internal resistance, enhance cell efficiency, and reduce costs. In general, rSOC has one supporting layer, which can support an electrolyte, anode, or cathode [30]. Planar designs are mostly anode-supported, while tubular ones are fabricated in electrolyte-supported configurations [31].

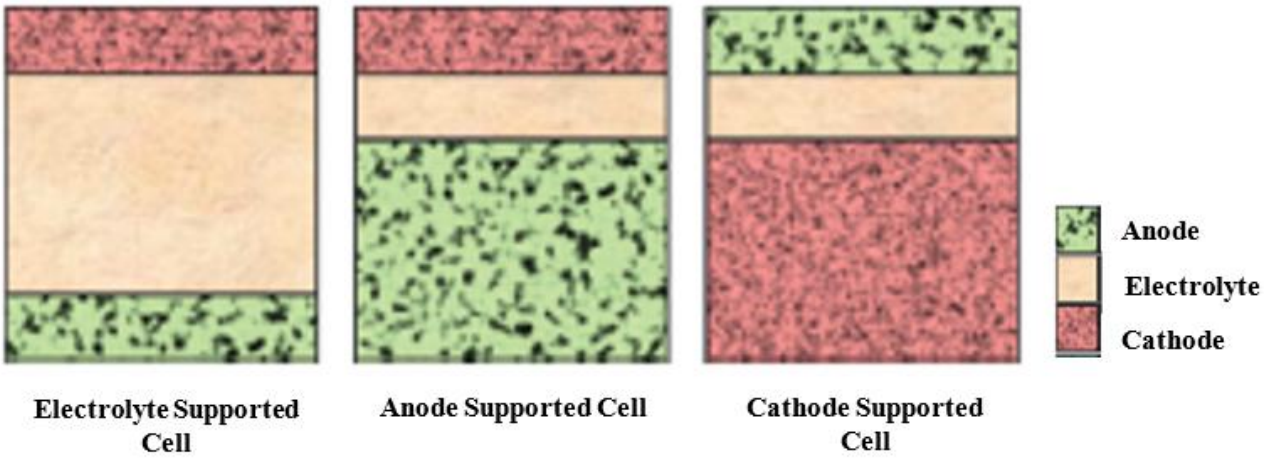

Figure 5: *Planar SOC with different support* [17]

Electrolyte-supported rSOC are the oldest design as YSZ provides a robust support layer and is easier to fabricate. However, a thick electrolyte layer causes higher ohmic losses, which degrades the power density output. Regarding the electrode-supported cells, an anode-supported design is more favourable than a cathode-supported one, owing to its higher power densities, particularly at lower temperatures. Furthermore, the anode-supported cells' fabrication process is simpler, and the anode microstructure is more controllable than that of cathode-supported cells.

Additionally, stacks comprise several SOC single cells linked by interconnects. Between the reducing and oxidising atmospheres of the anode and cathode, interconnects serve as a physical barrier[29]. In addition to collecting current and directing gas flows, interconnects are necessary for series stacking of several cells. Stacking enables the system to have a larger voltage when stacked in series or current when staked in parallel than a single cell [17]. In order to prevent leaks or the direct mixing of fuel and oxidant, planar design stacks need a sealant. On the other hand, sealing is often not a significant problem in tubular SOFCs [29].

It is worth noting that there is another geometry for SOFC stacks, the flat-tubular configuration, which provides the features of both planar and tubular SOFCs into a single design, like high power density, good thermal robustness, and ease of sealing [32]. Despite industry's interest in anode-supported cells, both anode and electrolyte-supported cells are used in laboratory experiments. For instance, in a three-electrode operation, the electrolyte support enables a simpler independent study of each electrode process, whereas the anode support provides better output results [31]. Forschunzentrum Jülich has been actively involved in the research and development of rSOC, particularly anode-supported cells, which have shown excellent stability during long-stack tests.

3.2 SOC Material

SOC stacks are operated at high temperatures, typically between 600°C and 900°C. Therefore, materials used in the stack should have excellent thermal and chemical stability at high temperatures [33]. The different SOC materials characteristics are discussed as follows:

3.2.1 Electrolytes

The electrolyte conducts oxygen ions between separated electrodes, which enables the overall reactions to take place. The oxygen vacancy hopping process is responsible for oxygen ion conduction. An essential factor that determines the SOC stack's operating temperature is the ionic conductivity of the electrolyte. The main requirements for the electrolyte in SOC are as follows:

- High oxygen ion conductivity (~ 0.1 Scm^{-1} at operating temperature)
- Low electronic transference number (< 10^{-3})
- Reliable mechanical properties
- Thermal and chemical stability from room temperature to ~1000°C at variable activities of oxygen (1 – 10^{-22}atm)

- Chemical inertness with electrode materials
- Compatibility of coefficient of thermal expansion (CTE) with cell components [33].

Many materials have been engineered to act as electrolyte materials. Zirconia-based (e.g., YSZ), ceria-based (e.g., gadolinia-doped ceria (GDC), and lanthanum gallate-based (e.g., $La_{0.8}Sr_{0.2}Ga_{0.8}Mg_{0.2}O_{3-\delta}$ (LSGM)). Yttria (3, 8, or 10 per cent) stabilised zirconia (YSZ) is SOC's most widely used material as a solid electrolyte. YSZ exhibits low electronic conductivity at temperatures above 700 °C while providing significant conductivity at these temperatures ([29], [34]). Another material, Scandia stabilised zirconia (ScSZ), has better stability and higher conductivity than YSZ. Prices and availability of Scandia are the major factors creating impedances in using this otherwise efficient material ([35], [36]).

Another interesting electrolyte material is Gadolinia-doped Ceria (GDC) or Cerium Gadolinium Oxide (CGO), which shows higher conductivity as compared to YSZ or ScSZ, specifically at low temperatures, reflecting a great potential for use in intermediate temperature SOC (IT-SOC). However, the challenges with using GDC are the mixed electronic and ionic conduction behaviour at low oxygen partial pressures, mechanical stability, cost and availability of Gadolinium [18]. One of the interesting electrolyte materials is perovskite-based Lanthanum Gallate ($LaGaO_3$) doped with Sr on the La-site and Mg on the Ga-site ($La_{1-x}Sr_x)(Ga_{1-y}Mg_y)O_3$ having high ion conductivity at low operating temperatures. A few factors limiting the use of this material are the evaporation property of Ga at low oxygen partial pressures, phase stability, mechanical stability and incompatibility with Nickel oxide (NiO), which is usually applied as the anode material [36].

It has been shown that solid electrolytes can be made to conduct protons. While these electrolytes are still in a very early stage of development, such proton conductors might eventually overcome some of the limitations of cells as oxygen ion conductors [25].

3.2.2 Fuel electrode

In SOCs, the fuel electrode breaks the H-H or H-O bond by catalysing the hydrogen oxidation reaction (HOR) in the SOFC mode and steam electrolysis in the SOEC mode. Therefore, the desired electrode materials should have high electronic and ionic conductivity, high electrocatalytic activity, chemical stability, high temperature under a reducing atmosphere, and good compatibility with other cell components ([33], [37]). The most popular hydrogen electrode material for SOCs is unquestionably nickel oxide because of its outstanding catalytic activity, electrical conductivity, and widespread availability. However, a mismatch between

pure Ni and the commonly used YSZ electrolyte weakens the attachment with the electrolyte ([18], [33]). Ni-YSZ cermet is currently the most widely used anode material due to electronic conductivity, good ionic conductivity and good catalytic activity toward hydrogen oxidation. The drawback of this composite is that it is susceptible to poisoning. Perovskites, such as titanate (doped $SrTiO_3$) and chromite (doped $LaCrO_3$), have been thoroughly studied as alternatives for new fuel electrode materials. The perovskite-type material has excellent tolerance for sulphur poisoning and carbon deposition and good structural stability but suffers from low catalytic activity and conductivity compared to Ni [18].

3.2.3 Air electrode

In SOCs, an air electrode catalyses oxygen reduction reaction (ORR) under SOFC mode and oxygen evolution reaction (OER) under SOEC mode, providing a pathway for ion migration and mass transportation. Therefore, materials are required to possess good electrocatalytic activity for ORR/OER and decent electronic/ionic conductivity or mixed ionic and electronic conductors (MIEC) and interfacial compatibility with the electrolyte. The air electrode should be sufficiently porous and maintain good stability under an oxidising atmosphere [38]. Given these requirements, metal oxides, particularly perovskite-based oxide of the general formula ABO_3, have become the most ideal and important material for air electrodes in SOC. A-sites are occupied by higher valence cations (La Sr, Ca, Ba etc.), while B-sites are occupied by higher valence-reducible transition metals (Ti, Cr, Ni, Co Fe etc.) [39].

The most frequent and typical air electrodes used in SOCs are lanthanum strontium manganite (LSM). LSM exhibits excellent chemical and structural compatibility with the majority of conventional electrolyte materials, as well as good catalytic activity towards ORR/OER. The main drawback with LSM is that it is primarily an electronic conductor with little ionic conductivity, which limits the ORR/OER reaction at the electrode/electrolyte/oxygen boundaries, i.e., triple phase boundary (TPB). The electrode performance with a single LSM component is insufficient for practical application. As a result, LSM is frequently used in conjunction with an ionic conductor, such as YSZ. Due to the reaction zone's extension from the electrode/electrolyte contact to the electrode bulk, the composite electrode (such as LSM-YSZ) displays improved electrochemical characteristics for the ORR/OER [18]. Alternative air electrode materials must be developed and optimised for SOCs operating in the IT regime (600-800), as the LSM itself does not seem to be a suitable option due to (at least in part) its low ionic conductivity and slow surface oxygen exchange kinetics. Lanthanum strontium cobalt

ferrite (LSCF) is the most representative and investigated MIEC electrode in intermediate-temperature SOCs [40].

LSCF is characterised by its high ionic conductivity and electronic conductivity at 800°C. LSCF's exceptional oxygen diffusion properties make it the most important and widely used MIEC electrode in SOCs. However, the application of LSCF in cells with YSZ electrolyte is limited because the CTE value of LSC is much larger than that of YSZ and the formation of the poorly conducting $La_2Zr_2O_7$ or $SrZrO_3$ phase at the air electrode/electrolyte interface. Therefore, a barrier layer (usually GDC) must be applied at the air electrode/electrolyte interface when LSCF is used with the YSZ electrolyte [33].

3.2.4 Interconnect and Protective coating

The interconnector provides a connection between adjacent cells in a SOC stack, through which the current and heat are conducted. Moreover, the interconnect also ensures the separation of fuel and air electrodes within the stack. An interconnect material typically needs to have high electronic conductivity with low ionic conductivity, thermal expansion compatibility with other cell components, high mechanical strength, high thermal conductivity, and chemical stability with regard to other cell components [35]. Ceramics and metallic alloys are the most common materials used as interconnect. The $LaCrO_3$-based ceramics have high electrical conductivity, which doping La with Ca or Sr can further be improved. Also, $LaCrO_3$ has a low coefficient of thermal expansivity mismatch with other cell components and is compatible with other components. However, using $LaCrO_3$ in SOC stacks is limited by its poor sinterability in air and reduced conductivity at intermediate temperatures. Therefore, metallic materials have become alternatives for interconnectors in SOC stacks running at intermediate temperatures (650°C to 850°C) [33]. Currently, a variety of metallic materials have been created for metallic interconnectors in SOC stacks, including ferritic stainless steel, Ni-based alloys, and Cr-based [41]. Ferrite stainless steel shows similar CTE to other stack components with a relatively simple manufacturing process. As a result, ferritic stainless steel has emerged as the SOC stack's most popular interconnector material. Crofer22 series ferritic stainless steel was developed at the Research Centre Jülich in Germany and commercialised by ThyssenKrupp VDM in Germany. It has become the most commonly used interconnector material because of its potent antioxidant qualities and excellent high-temperature conductivity [33].

Since volatile Cr element generated from the Cr_2O_3 scale layer can easily deposit and poison the oxygen electrode, leading to irreversible cell performance degradation. One of the common

methods to suppress Cr volatilisation is to apply a dense protective layer to the surface of the interconnect material [18]. For the Jülich stacks, manganese cobalt ferrite (MCF or (Mn, Co, Fe_3O_4) is used as the standard protective coating on the Crofer 22 APU interconnector.

3.2.5 Sealants

In a SOC stack, sealant material helps to keep the fuel gas and air separate in their respective chambers and prevent the two from mixing. In tubular design, sealant is unnecessary as the stack is self-sealing. However, the planar design's performance is highly related to sealing conditions [33]. According to the specific working conditions of SOCs, the sealants must be cost-effective, have high hermeticity, long-term stability in air and reducing environments, be chemically compatible (no or minimal chemical interactions), thermal expansion compatible with the surrounding components, and intrinsic insulating and cost-effective [18].

Various types of sealant materials have been developed and used for SOC stacks, including metal, brazes, glass, glass-ceramic, and mica-based composites [42]. The sealing methods employed in SOC stack sealing determine material selection [33]. In a compressive seal, the sealant material is inserted between the two sealing surfaces, and external compressive stress is applied to the sealing surfaces to create a gas-tight seal. The CTE matching is not necessary for the sealant material because it is not bonded to the components of the next stack. The sealant material must be flexible enough to distort and produce compression. The two sorts of materials that meet these standards are those made of metals and those based on mica [33]. Among metallic materials, noble metals particularly Ag, are the most appropriate sealant due to their high melting point, strong degradation resistance and cost-effectiveness. The problem with using Ag as a sealant material is the insufficient deformability due to high yield strength.

Furthermore, water formation in the sealant has been observed due to the high solubility of Hydrogen and Oxygen in Ag. Muscovite ($KAl_2(AlSi_3O_{10})(F,OH)_2$) and phlogopite ($KMg_3(AlSi_3O_{10})(OH)_2$) are the two main types of mica used as sealants. However, the pure mica sealant shows a high gas leakage rate. The hermicity of pure mica can be improved by improving the thickness and combining it with other materials [43].

Compared to compressive sealing, rigid sealing is significantly easier and more efficient since the sealants are bonded with the sealing surfaces [43]. Instead of compressive sealing, which is necessary to prevent significant thermal stress during thermal cycling, CTE matching between the sealant material and neighbouring stack components is needed. Glass, glass-ceramic, and braze materials with alloy bases are among the sealant materials utilised for hard

sealing. Glass possesses a relatively higher CTE value but lower strength than ceramic material. The commonly used glass-ceramic sealant materials for SOCs are borosilicate glass, boron-free alkaline earth silicates, and phospho-silicate glass [33]. The standard sealant used in the Jülich stack is the glass matrix of the BaO-CaO-SiO_2 system with additions of Al_2O_3, B_2O_3, ZnO and V_2O_5 (Glass H). The glass matrix is usually filled with YSZ fibres or Ag particles. Currently, the joining process of the SOC stack is performed at 850 °C for 100 hours to ensure that the sealant obtains a partial crystallisation microstructure with sufficient mechanical stability [33].

4 Degradation Mechanism

The key variable affecting the commercialisation of SOC technologies is the durability of SOC stacks. Thus, the main challenge in SOC research and development is to extend the stack and system lifetime. Numerous studies have been conducted on the degradation of SOC stack operated in SOFC and SOEC to determine the degradation origin and the relevant mechanism ([33], [44]). Degradation of SOC is described as the loss of performance over time. In most cases, the degradation rate is expressed as the voltage loss per 1000 hours or the change in area-specific resistance (ASR). Assessing the degradation process and mechanism is a complicated process.

Moreover, SOC stack degradation depends on material and operating conditions such as temperature, fuel impurities, and current density ([29], [44]). The combined and complex nature of SOC degradation requires a methodical approach. A deconvolution of this problem is identifying degradation phenomena arising from the different components, as shown in Figure 6. Components critical in the overall SOC degradation are discussed below.

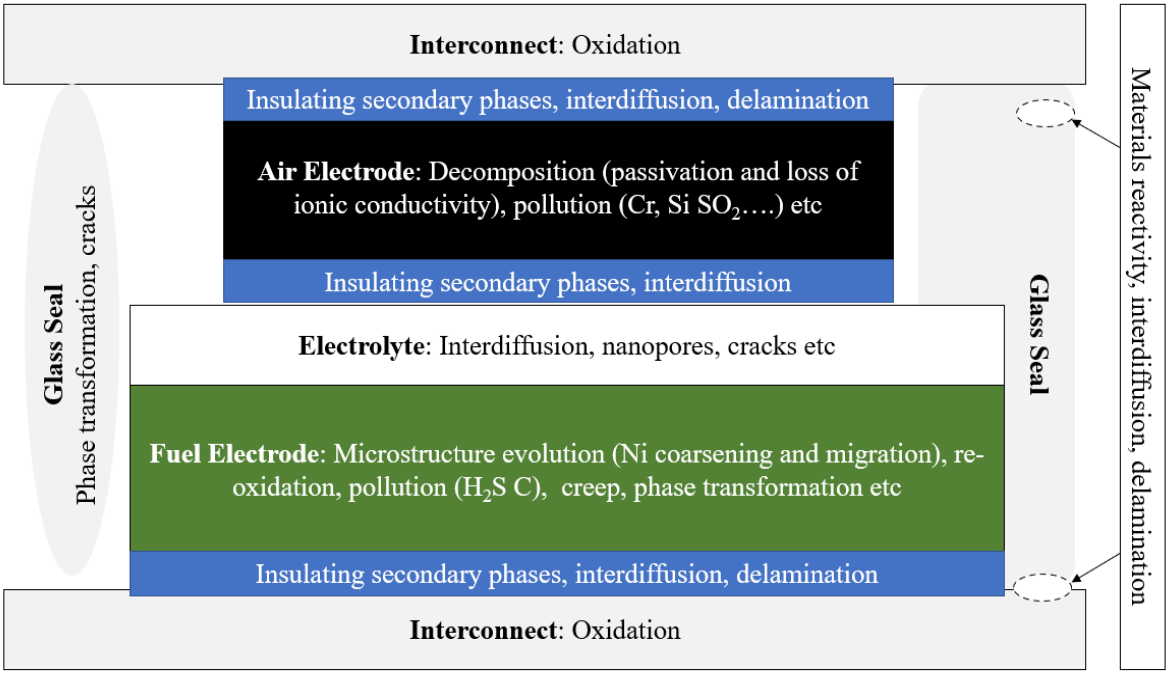

Figure 6: *Degradation phenomena in different SOC components* [10]

4.1 Fuel Electrode

The main source of degradation of an electrode-supported (Ni-YSZ) SOC during operation in both SOFC and SOEC modes concerns microstructural changes in the Ni network ([10], [29], [44]). Common microstructure change that has been observed under reversible operation is Ni migration and coarsening or agglomeration of Ni particles, which decreases the total TPB length ([7], [10]). The difference between Ni particle size was considered to be the driving force for the growth of larger Ni particles, and the Ni atom surface diffusion was the dominant diffusion mechanism. Ni coarsening decreases TPB length, increasing polarisation resistance [37]. Ni coarsening has been reported for both SOFC and SOEC operations. Ni agglomeration generally occurs independent of the operating mode due to high operating temperatures and the specific operating environment. It can appear even under OCV because of material instability during long-term operation, and this degradation phenomenon cannot be prevented as the operating time increases. However, specific operating conditions, such as temperature, steam concentration and, in general, fuel composition, can significantly accelerate Ni-agglomeration [7].

By diffusion and evaporation/condensation, Ni coarsening can also cause Ni to migrate to the anode surface. The reaction of Ni, O_2, and H_2O to create $Ni(OH)_2$ occurs close to the TPB zone under the operating conditions of the SOFC, which include high temperature and steam

pressure. $Ni(OH)_2$ would evaporate, be transported to the surface, and then condense to Ni atom because it has a lower melting point than the operating temperature. The oxygen partial pressure of O_2 at the fuel electrode side increases with the steam/H_2 ratio in the electrolysis mode. The creation of nickel hydroxide and the transport of nickel to the surface would be accelerated, resulting in greater nickel agglomeration and evaporation than in fuel cell mode [33].

Another microstructural change that takes place in the case of redox cycling is a severe cause of Ni-YSZ cermet degradation in terms of both electrochemical and mechanical performance. Although reoxidation should not occur under well-controlled working conditions, during long-term operation, it is an expected but unpredictable phenomenon due to excessive oxidising species that can diffuse to the fuel electrode as a result of leakage, fuel starvation, and increased oxygen partial pressure. It can be caused by high fuel utilisation during SOFC operation or low steam utilisation during SOEC operation ([7], [10]).

Besides microstructural change, SOC enjoys fuel flexibility because of high working temperature. This makes it possible to use non-hydrogen fuel gases like hydrocarbon carbon monoxide and ammonia fuels [33]. However, carbon deposition occurs when carbon monoxide from the reforming process reacts with H_2, resulting in the degradation of the fuel electrode. The risk of carbon deposition at the fuel electrode is increased because the oxygen is carried away from the fuel electrode to the air electrode. However, the deposition mainly occurs at the fuel electrode/electrolyte interface rather than on the electrode surface observed during fuel cell operation. The deposited carbon will block the active TPB and destroy the electrode structure. Traces of impurities in the fuel gas, such as sulphur chlorine, also lead to stack degradation [37]

4.2 Air Electrode:

Different materials with different conductivity types have been developed for the oxygen electrodes in SOCs. Because of the excellent chemical and thermal compatibility with YSZ, LSM is the common material for SOC air electrodes [33]. Degradation mechanisms that have been observed for LSM-based air electrodes include delamination and formation of zirconate at the LSM/YSZ interface while the cell operates at low temperatures due to the high overpotential on the LSM air electrode and the low oxygen activity at the interface. Interface densification, monoclinic formation and Mn oxide exsolution are observed at high temperatures after operation [44].

Zirconate formation is observed at the LSM/YSZ interface under fuel cell and electrolysis operation. The formation of this poor conductive zirconate will weaken the contact between the air electrode and electrolyte and increase the overall ohmic resistance. Delamination of the air electrode at the air electrode/electrolyte interface due to the local high oxygen chemical potential under anodic overpotential is the most common LSM air electrode degradation process in SOEC [33].

When using Crofer 22 series stainless steels as interconnector materials, the formation of volatile species such as CrO_3 or $Cr_2(OH)_2$ in the presence of water reacts with $LaMnO_3$-based air electrode, which further participates in the ORR process at TPB, leading to the formation of Cr_2O_3. Cr_2O_3 is then deposited in the air electrode interface, which can seriously degrade the air electrode performance [33].

LSC and LSCF are alternative air electrode materials having high electronic conductivity and as well as high oxygen ion conductivity. However, Sr surface segregation and Co segregation have been reported as the degradation mechanism of the electrode material [45]. With the anodic polarisation under electrolysis mode, SrO segregation is accelerated, resulting in the formation of SrO on the surface of the air electrode surface and the Sr/Co depletion inside the electrode.

4.3 Electrolytes:

The main degradation mechanisms are grain interior dopant segregation and kinetic demixing, grain boundary dopant segregation, phase instability, and order-disorder transformations. These phenomena decrease the concentration of oxygen vacancies or reduce oxygen vacancy mobility by forming defect associates (oxygen vacancy is bound to the dopant, impurity, or cation) or creating elastic strain (pinning the oxygen vacancy). [44]

When the SOC operates in electrolysis mode, the oxygen activity at the fuel electrode/electrolyte interface decreases but increases at the air electrode/electrolyte interface. Therefore, the oxygen activity at the two interfaces is divergent, increasing the oxygen activity gradient across the cell. In the electrolyte/air electrode interface, the oxygen activity in the electrolyte can exceed the standard free energy of oxygen formation, therefore allowing oxygen formation. Based on this mechanism, the oxygen ions from the hydrogen electrode can form oxygen bubbles in the YSZ grain boundaries close to the air electrode ([44], [46]). Consequently, it will lead to damage and internal fracture formation in the electrolyte near the air electrode, which can increase ohmic resistance.

4.4 Interconnect:

Despite playing no active part in the electrochemical reaction, interconnects are essential to SOC stacks due to the necessary characteristics and operating conditions they must withstand. Their exposure to simultaneously oxidising and reducing atmosphere, SOC temperature and direct contact with electrodes introduce degradation sources [10]. Figure 7 shows a breakdown of the metallic interconnect degradation process.

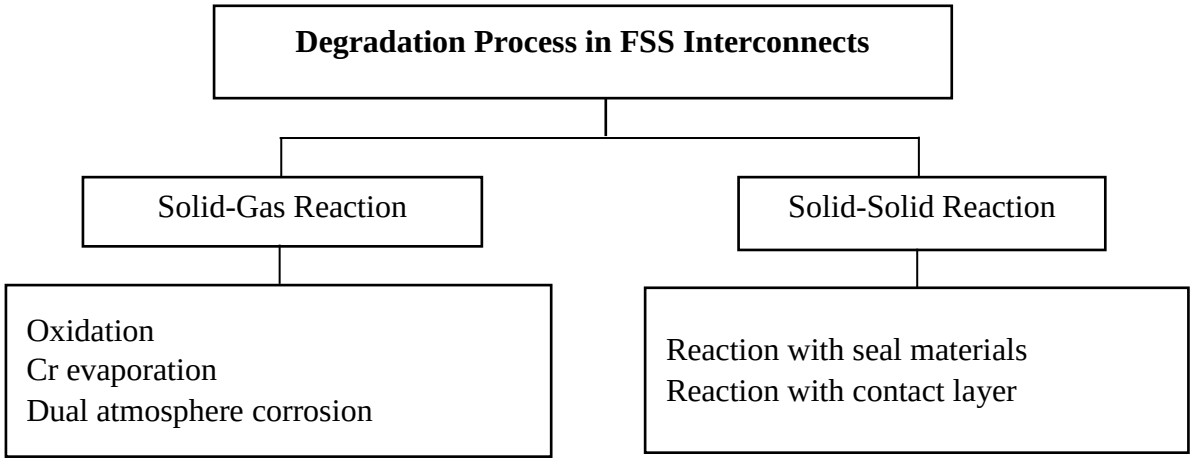

Figure7: *Degradation mechanism in metallic interconnects (Adapted from [10]).*

Croffer 22 series ferrite stainless steel is the most commonly used material owning to good antioxidant properties due to Cr_2O_3 protective surface scale. However, the Cr_2O_3 is oxidised at high temperatures, leading to the emergence of $(Mn,Cr)_3O_4$, reducing electrical conductivity and the mechanical stability of interconnects. Moreover, the simultaneous exposure to fuel on one side and air on the other is another cause of the corrosion, called the "dual atmosphere effect"[29]. Cr vaporisation from interconnects in wet air conditions of SOC causes Cr poisoning in the cathodes, one of the most severe degradation mechanisms responsible for a significant decrement in electrical conductivity by blocking the electrode's active TBP sites ([10], [47]). Furthermore, this Cr vaporisation induces the Cr depletion in the interconnect, and this depletion below a specific threshold threatens its mechanical strength and structural integrity through the oxidation break-away [10].

Conclusion

Reversible Solid Oxide Cell (rSOC) is an electrochemical device that can produce heat, electricity and valuable chemical in a single unit. They have a range of desirable properties compared to low-temperature fuel cells and electrolysers. However, degradation challenges impede their wider commercial adoption. Several factors cause SOC stack degradation, and most degradation phenomena are closely related to the operating conditions, including operating temperature, the degree of reactant utilisation, operating current densities, fuel used, composition and impurities.

CHAPTER II:

METHODOLOGY

CHAPITER II: METHODOLOGY

INTRODUCTION

This section provides a detailed explanation of SOC stack experiments and SOC degradation measurement techniques. The following section will also discuss a detailed description of what constitutes a load operating phase and the statistical methods to identify the main contributors to SOC degradation.

1 Reversible Solid Oxide Cell System Description

The general composition of the rSOC stacks used in this analysis includes:

- Fuel Electrode: Ni- YSZ cermet
- Air Electrode: LSCF or LSC
- Electrolyte:8YSZ
- Contact anode: Ni-Mesh
- Interconnects: Crofer 22APU
- Sealant (Stack): Glass 87 ZYBF-2
- Sealant (adapter Plate): Mica

The full description and function of the components has been explained in section 3.2

1.1 Description of Stack Experiments

The experimental data for this analysis were drawn from different stack tests assembled according to the Julich F10 design. The cell has an overall area of $10cm \times 10cm$ and an active area of $80cm^2$.The cells were anode-supported (in SOFC mode) made of Ni-YSZ as the fuel electrode, 8YSZ as the electrolytes and LSC or LSCF as the air electrode. Each stack contains two or more layers of cells (Elcogen cells) joined together using a glass sealant. Figure 8 shows the schematic of the stack test mounted on the test bench. The test bench is equipped with a measurement and controlling device where SOC operation can be monitored and controlled. During SOC stack tests, an automated data acquisition method was used to record the operating conditions of the stack, such as stack temperature, fuel flow rate, air flow rate, voltage etc. IV curve measurement and EIS measurement are also conducted during stacks tests are recorded. The data were consolidated and stored as an HDF5 file

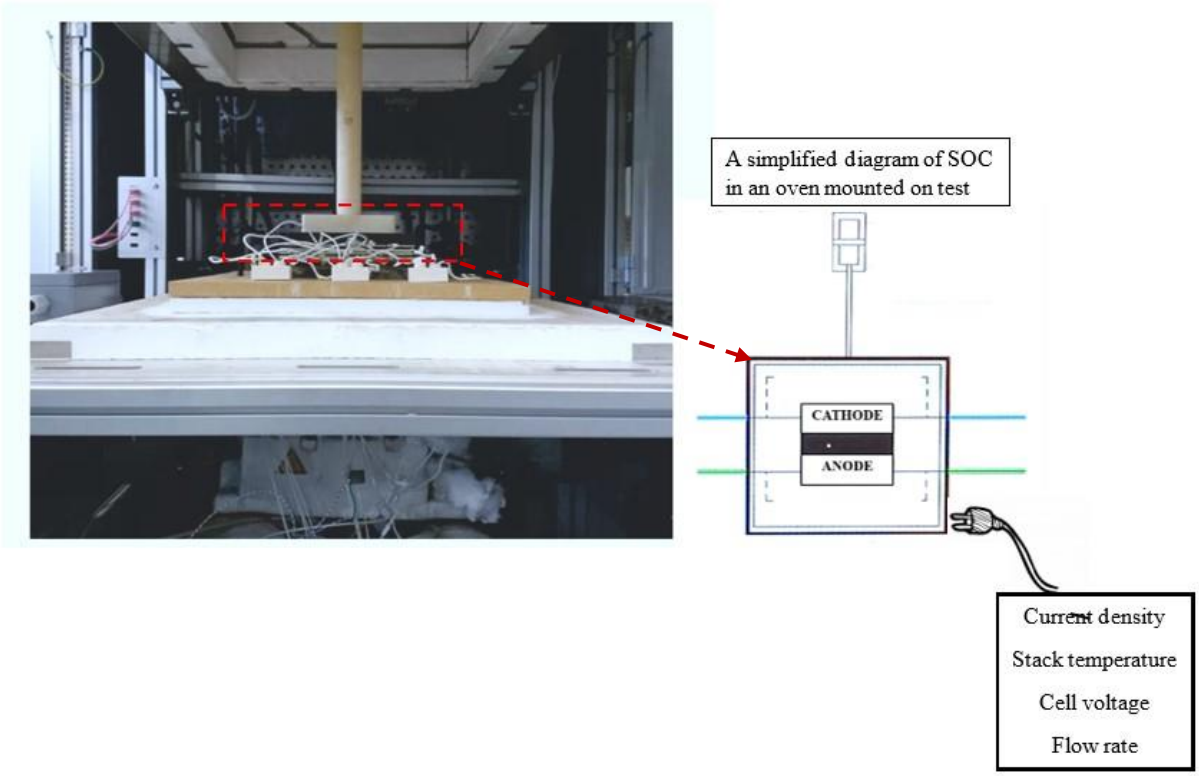

Figure 8: *SOC stack mounted on a test bench*

2 Method

2.1 Identification of Load Phases

The time trace of each stack experiment was read using Pandas library in Python. The time trace data were plotted and visualised to get an overview of what was done in the experiments. Different load operating phases were identified for each stack experiment. A load operating phase is a region or specific stage of steady operation where the cell generates electrical energy in the context of an SOFC. In SOEC, load operating is a region or specific stage of steady operation when an electric current is applied to the cell. Figure 9 shows a different load operating phase identified for stack experiment SK672-F1004-102 under SOFC operation.

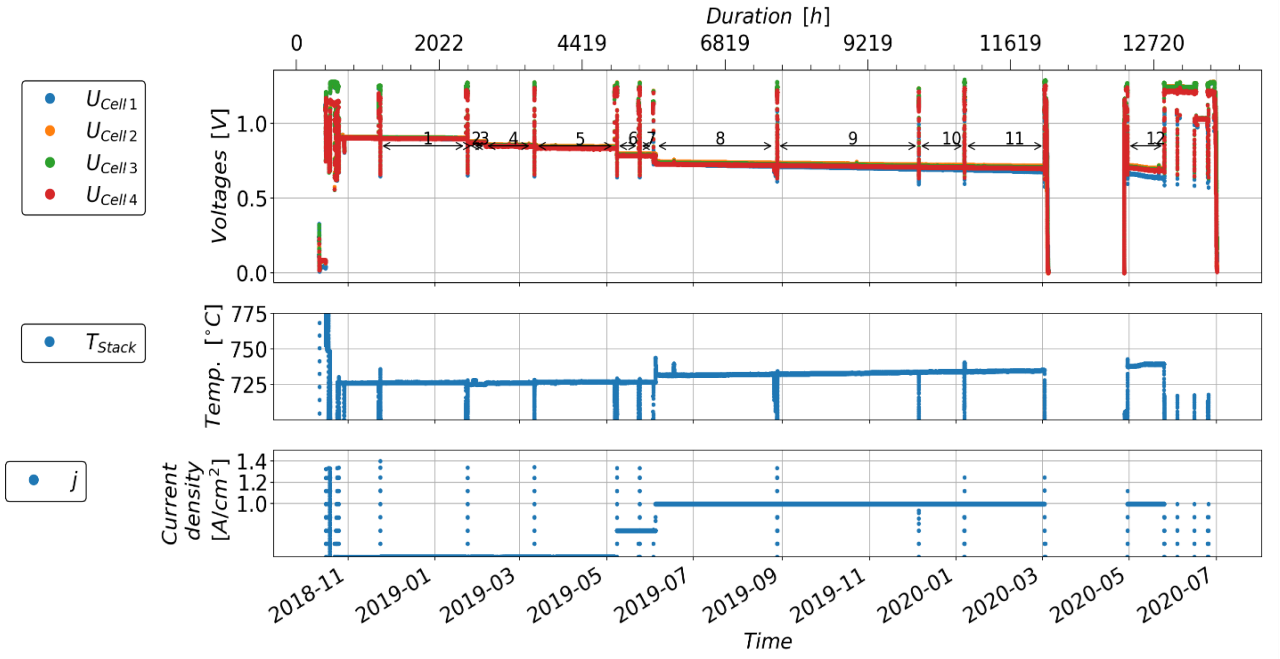

Figure 9: *Time trace plot with identified load phases*

2.2 Calculation of Degradation Rate for each Operating Load Phase

The degradation rates for each phase were computed after various load operating phases from various stack experiments were identified. Figure 10 illustrates how the cells' voltages decrease with time, indicating that the cells are degrading during SOFC operation. In calculating the degradation rate for each phase, a regression was fit through the data point obtained from the plot of voltage measurement over time. The Huber Regressor algorithm was used to fit a regression line through the data point. Huber regression algorithm model has the advantage of not being heavily influenced by outliers in the data point but also not wholly ignoring their effect. This regression line takes the form of a straight-line equation represented as:

$$U(mV) = mx + C \qquad \text{II.1}$$

Where:

U= voltage at any specific point in time

$x =$ time (independent variable)

$m =$ slope of the regression line, which indicates the degradation rate.

$C =$ intercept.

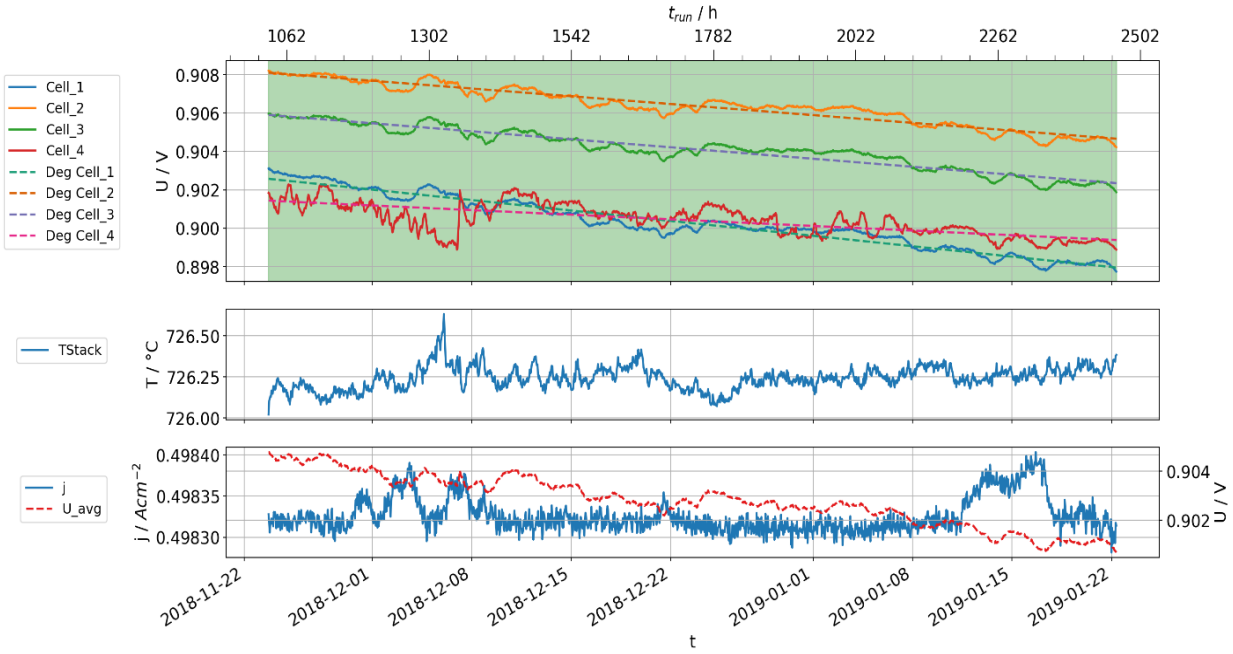

Figure 10: *Degradation Rate calculation using Regression Algorithm*

The degradation rate estimation was done for all the phases identified in all the stack experiments considered for this analysis. The operating conditions, such as stack temperature, current density and conversion rate describing the phases, were collected and tabulated accordingly.

2.3 Probabilistic Modelling

In statistics, models are simplified descriptions of a given system or process we are interested in for any purpose. The statistical model helps us understand and make predictions given some observed data. Different models exist and are used for different purposes and statistical analysis. In the context of this research, the Bayesian regression model, also known as a probabilistic model, is used to identify the main contributors to SOC. Linear regression is a common statistical method for modelling the relationship between a dependent and one or more independent variables. This model helps us understand if there is a linear relationship between the dependent and independent variables, how strong the relationship is, and which dependent variable has a strong effect (James et al., 2013). Mathematically, we can write this linear relationship for a dependent (response) variable Y and independent X as:

$$Y \approx \beta_0 + \beta_1 X \qquad \text{II.2}$$

Equation II.2 suggest that there is a linear relationship between the variable X and Y. This is the case of simple linear regression. Equation II.2 can be extended to a case of multivariate linear regression where there is more than one independent variable. Then the model becomes.

$$Y \approx \beta_0 + \beta_1 X + \beta_2 X_2 + \beta_3 X_3 + \cdots + \beta_n X_n \quad \text{II.3}$$

In practice, $\beta_0$is the intercept and $\beta_1, \beta_2, \ldots . \beta_n$ correspond to the slope quantifying the association between the independent and response variables [50]. These unknown parameters are the model parameters or coefficients we need to determine such that any given input variable produces a predicted response variable. Finding the parameters of the linear regression model can be done in a few ways, one of which is Least square fitting. The least squares return the values of the unknown model parameter, yielding the lowest average quadratic error between the observed and the predicted. When put in this way, the problem becomes an optimisation problem, determining the minima or maxima of a function. Rather than using this traditional optimisation approach, which returns a single point estimate, Bayesian linear regression provides a powerful and flexible approach by incorporating the Bayesian principle that helps us to obtain the best value of the model parameters together with an estimation of the uncertainty we have about the parameters' value [49].

In a Bayesian viewpoint, linear regression is formulated using probability distribution rather than point estimates, where the response variable is assumed to be drawn from a probability distribution. Bayesian linear regression sample from normal distribution has the form:

$$y \sim N(\beta^T X, \sigma^2 I) \quad \text{II.4}$$

y in Equation II.4 is generated from a normal (Gaussian) distribution described by a mean and a variance. The mean of the linear regression model is the transpose of the coefficient matrix multiplied by the matrix of the predictor. The variance is the square of the standard deviation multiplied by the identity matrix, given that this is a multi-dimensional model formulation. Since we are interested in estimating unknown model parameters, the model parameter is assumed to come from a form of distribution as well. The posterior probability of the model parameters is upon the training input and output using Bayes Theorem [51].

$$P(\beta|y,X) = \frac{P(y|\beta,X) \times P(\beta|X)}{P(y|X)} \quad \text{II.5}$$

$P(\beta|y,X)$=The posterior probability distribution of the model parameters given the input X and output y.

$P(y|\beta,X)$= The likelihood of the data.

$P(\beta|X)$ =The prior probability of the model parameters.

$P(y|X)$ =The normalizing constant.

2.3.1 Prior

Priors represent the background knowledge of the model's parameters to estimate. It is the first component in Bayesian statistics that represents our knowledge before seeing the data. It is usually captured in a distribution called prior distribution with parameters such as mean and variance depending on the type of distribution. The variance of the prior distribution shows the level of uncertainty about the population of the value of the parameter of interest. That is, the larger the variance, the more uncertain we are. Prior distribution can be informative or noninformative [52]. When we do not know anything about the population of the parameters to be estimated, it is called noninformative priors. Therefore, values within the distribution are equally likely. We have an informative prior distribution when we incorporate what we already know about the parameters to be estimated by specifying the mean and the variance. By selecting an appropriate prior, regularisation can also be achieved in the Bayesian contexts.

Regularisation is a technique used to determine relevant predictors when there are several potential predictors in a multivariate regression by shrinking the ineffective covariates towards zero, which does not contribute to the predictors [53]. Hierarchical regularised horseshoe prior is a typical regularisation that uses Global and local strategies to shrink model parameters to zero by applying a penalty to the size of the regression parameters. Equation II.6 is a horseshoe prior for each regression coefficient.

$$\beta_i \sim N(0, \tau^2 . \tilde{\lambda}_i^2) \quad \text{II.6}$$

τ is the global shrinkage parameter and $\dot{\lambda}_\iota$ is the local shrinkage parameter

$$\tau \sim Half\_StudentT_2(\frac{D_0}{D-D_0} . \frac{\sigma}{\sqrt{N}}) \quad \text{II.7}$$

$$\tilde{\lambda}_i^2 = \frac{c^2 \tilde{\lambda}_i^2}{c^2 + \tau^2 \tilde{\lambda}_i^2} \quad \text{II.8}$$

σ is the prior on error standard deviation, N, D is the number of predictors, and D_0 is the number of true non-zero coefficients usually given as $D/2$. To complete this specification, Half_StudentT5 and Inverse Gamma are used as the prior distribution for $\tilde{\lambda}^2$ and c^2 respectively [53].

2.3.2 Likelihood

This is the observed evidence expressed in terms of the likelihood function of the data given the parameters. In probabilistic terms, the likelihood is the probability of observing the data in hand given a set of parameters. The likelihood functions reflect the most likely value for the unknown parameters given the data.

2.3.3 Posterior

The posterior distribution is the third component in Bayesian statistics, combining the prior and likelihood. It reflects updated knowledge of the parameter of interest after observing the data. The posterior distribution is usually obtained using the Markov Chain Monte Carlo method [52].

2.4 Implementing Probabilistic Programming using PyMC3

PyMC3 is a new open-source Probabilistic Programming framework written in Python that uses Theano to compute gradients via automatic differentiation as well as compile probabilistic programs on the fly to C for increased speed. Probabilistic programming (PP) allows for flexible specification and fitting of Bayesian statistical models[53]. The following steps were taken to build a multivariate regression model for this analysis.

Step 1: Python and PyMC3 Installation

Running a PyMC3 for probability programming requires a Python interpreter. Python and the necessary data manipulation and visualisation library were installed, such as Numpy pandas and Matplotlib with Anaconda Python Distribution. Another Environment called "pymc" was created, and PyMC3 was installed following the installation guide on the PyMC3 documentation guide.

Step 2: Launch of Python

Using the Anaconda Navigator, I launched Python and created a Jupyter Notebook used for analysis. Numpy, Pandas and Matplotlib libraries were imported, and the consolidated table containing the different load operations from the stack test experiment was read using the Pandas library.

Step 3: Data Loading and Data Manipulation

After reading the data, the table was transformed to access the columns quickly. Additional columns were created, such as the mean degradation rate, resistance degradation rate and the mean degradation rate. In order to consider both electrolysis and fuel operation jointly for this analysis, the Fuel Utilization and Steam Utilization were combined into a single column as conversion rate. The current density for electrolysis mode and degradation rate for fuel operation were then defined in their absolute values for better comparison.

Step 4: Selection of Operating Parameter for Analysis

Variable selection was made, and the probabilistic model's necessary module was imported.

Step 5: Model Specification

The first step in specifying the model is to create a model object to serve as a container for the model random variable. Once the model object was created, the "with statement" was used to add a random variable. The prior distribution and the likelihood distribution of the model were specified.

Step 6: Model fitting

Once the model has been specified, the "sample function" was used to fit the model by drawing the sample from the posterior distribution with a maximum likelihood estimate.

Step 7: Posterior Analysis

Posterior analysis was done to ensure convergence during sampling.

Step 8: Posterior Distribution of Predictor Coefficients

After the convergence of the sampling technique, the "plot_forest function" was used to plot the Highest Density Interval (HDI) of the posterior distribution of the predictor coefficients to determine the relevance of each operating condition contribution to SOC degradation.

CONCLUSION

Load operation which corresponds to a region or specific stage of steady operation where the cell generates electrical energy in the context of an SOFC, while in the context of SOEC, the cell performs an electrolysis process when an electric current is applied has been identified and the degradation rate with the corresponding operating parameters (current density, conversion rate and stack temperature) were tabulated accordingly. A Bayesian multivariate regression model was used to investigate the main contributors in SOC degradation.

CHAPITER III:

RESULTS AND DISCUSSION

CHAPTER III: RESULTS AND DISCUSSION

INTRODUCTION

This chapter presents the result of the different load operations for different stack experiments analysed. The outcome of the Bayesian regression model will also be presented.

1 Results and Discussion

1.1 Identified Load Operation for Different Stack Experiments

A total of twelve stack test experiments with similar or homogenous material properties and configurations were considered for this analysis. The different load operating phases in each stack test experiment and the operating conditions for the load operating phases have been identified and tabulated accordingly.

Table 1 shows the load operations, degradation rates and corresponding operating conditions collected from Twelve (12) different stack experiments. A total of twelve load phases were identified for the **SK672-F1004-102** stack experiment. The third load phase, operated at a current density of 0.5Acm^{-2}, 60% fuel utilisation rate and a stack temperature of 725°C, exhibited improved performance rather than experiencing degradation during fuel cell operation. The load phase before this phase had similar operating conditions, but it was seen to undergo degradation. Improved cell performance was observed for Cell 3 for the stack experiment **SK706-F1004-111** under fuel cell operation. **SK709-F1005-15** stack experiment also exhibited an improved performance during fuel cell testing. Cell 1 in the **SK713-F10040-123** in the second and third fuel cell load operation also exhibited improved performance.

In the stack experiment **SK708-F102-197**, even though the different load phases identified were operated under the same operating conditions -0.5Acm^{-2}, 50% steam conversion and stack temperature of 747°C, the phases have different degradation rates. **SK714-F1004-110** stack experiment was tested for electrolysis operation Cell 1 and Cell 2 during the second load operation operated at a current density of -1.45Acm^{-2} and 80% steam conversion exhibited improved performance. The same was experienced for the stack experiment **SK729-F1004-124**, during which the fourth and sixth load operations, all the cells in the stack experienced improved performance.

Table 1: Load operation and corresponding operation condition

Experiment	Phases	Current density	Fuel utilization	Steam utilization	Stack temperature	Mean Voltage Cell_1	Mean Voltage Cell_2	Mean Voltage Cell_3	Mean Voltage Cell_4	Degradation Rate Cell_1	Degradation Rate Cell_2	Degradation Rate Cell_3	Degradation Rate Cell_4	Operating Time
SK672_F1004_102	1	0.498326	39.866087	NaN	726.244446	0.900263	0.906386	0.904127	0.900411	-0.003234	-0.002405	-0.002484	-0.001436	59 days 15:34:59.986373
	2	0.497829	59.953559	NaN	724.90271	0.874255	0.879248	0.876235	0.872091	-0.015104	-0.012618	-0.012382	-0.002049	3 days 21:04:59.422394
	3	0.497838	59.95465	NaN	724.92157	0.873588	0.878666	0.875623	0.871971	0.00521	0.00531	0.004831	0.005123	6 days 17:24:59.443222
	4	0.497842	74.8433	NaN	726.034058	0.855004	0.858103	0.853492	0.849237	-0.003288	-0.003146	-0.00396	-0.00338	31 days 23:59:59.929423
	5	0.5	80.57554	NaN	725.5	0.845099	0.847316	0.841128	0.836049	-0.002206	-0.001945	-0.002309	-0.003103	50 days 16:26:28.086304
...	...	...	...	...	...	...	...	...	...	...	...	...	...	...
SK755_F1002_198	2	-0.500125	NaN	49.788575	698.677784	1.189298	1.173989	NaN	NaN	0.013176	0.015039	NaN	NaN	5 days 19:43:29.965000
	3	-0.500125	NaN	49.788575	699.347489	1.194583	1.180411	NaN	NaN	0.015517	0.018518	NaN	NaN	10 days 17:16:11.664000
	4	-0.500125	NaN	49.788575	698.904661	1.197237	1.184158	NaN	NaN	0.011478	0.012433	NaN	NaN	18 days 17:04:09.918000
	5	-0.500125	NaN	25.010075	696.141603	1.10395	1.098858	NaN	NaN	0.011478	0.012433	NaN	NaN	25 days 14:51:49.301000
	6	-1.000125	NaN	50.013903	699.834389	1.373276	1.365	NaN	NaN	0.037472	0.039325	NaN	NaN	28 days 11:45:43.948000

1.2 Regression Analysis with Uninformative Priors Using Voltage and Resistance Degradation Rate as The Regressand

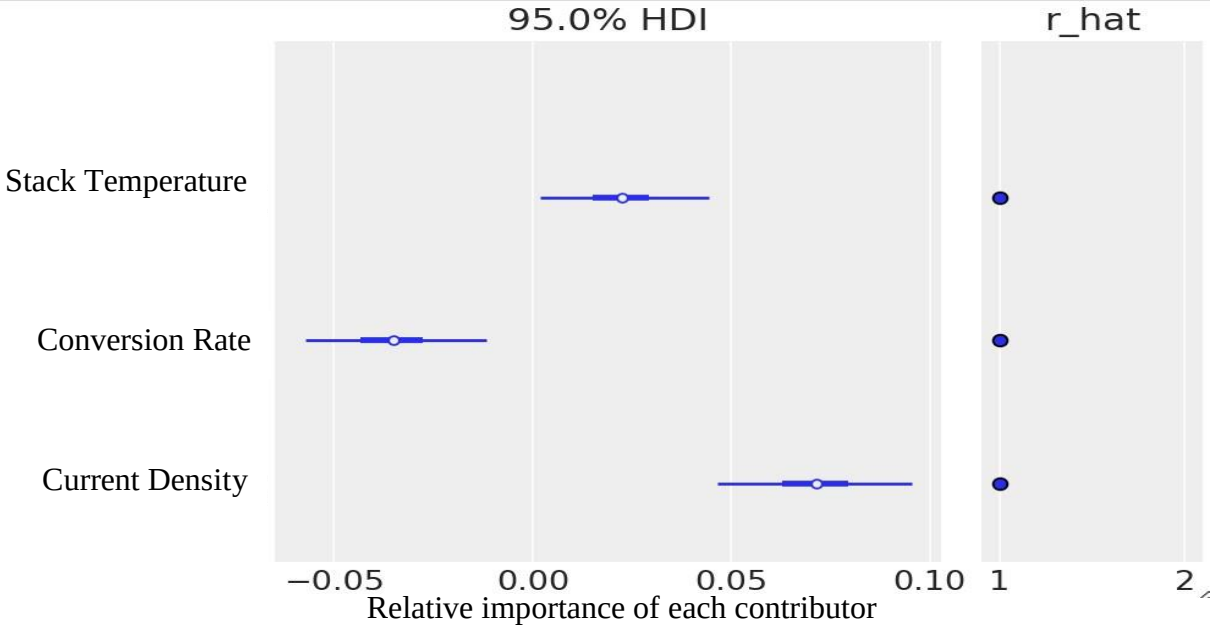

Figure 11:*Posterior Distribution of Predictor Coefficient with Voltage Degradation Rate as the Regressand*

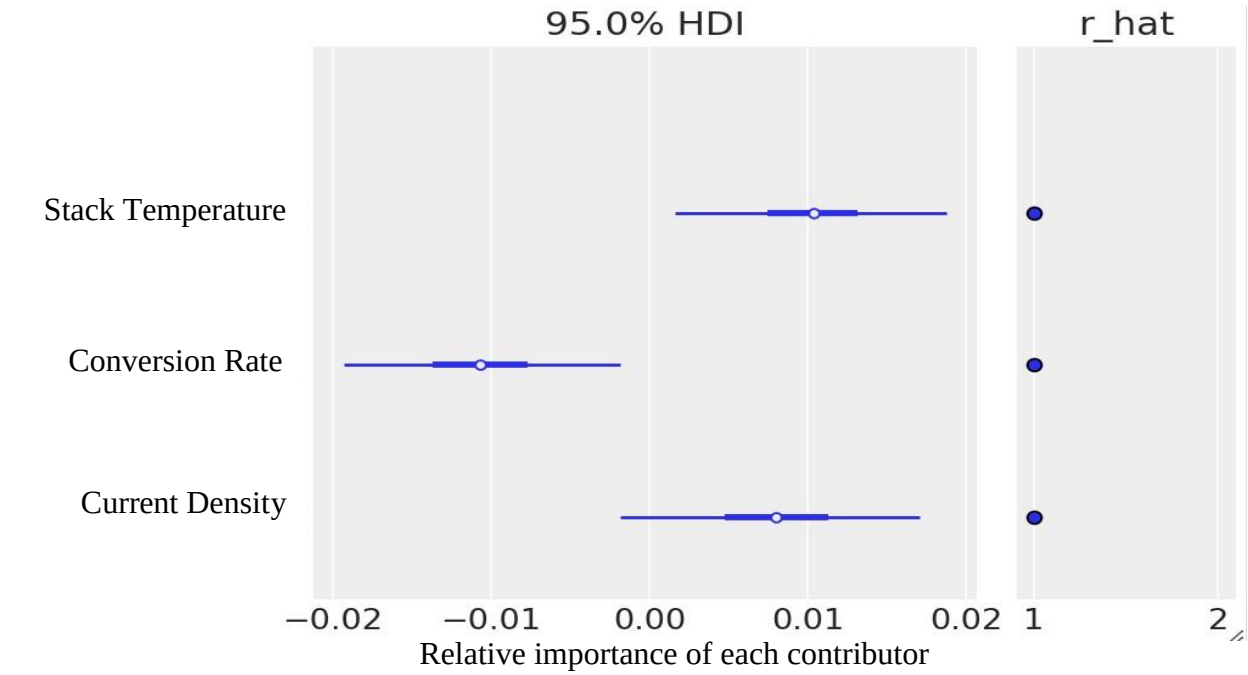

Figure 12: *Posterior Distribution of Predictor Coefficient with Resistance Degradation Rate as the Regressand*

The outcome of multivariate Bayesian regression with normal priors with the Highest Density Interval (HDI) of the set of predictors is shown in Figures 11 and 12. The HDI summarises the distribution by specifying an interval spanning most coefficient regressions by 95%. The posterior distribution of the coefficient of the regressor reveals which factor contributes to SOC degradation. According to Figure 11, current density has a positive and an absolute value more significant than all other regressors. This indicates that the current density contributes to SOC degradation the most. Increasing the current density will lead to a larger increase in the degradation rate of SOC stacks.

On the other hand, the conversion rate is negative and has an absolute value smaller than the current density, which is a second contributory factor that affects the degradation rate in SOC. The result indicates that increasing the conversion rate leads to a decrease in degradation rate while decreasing the conversion rate leads to an increase in degradation rate. This particularly seems to contradict what has been observed from experiments. Fang et al. [14] reported that increasing the conversion rate increases the degradation rate. Another separate study, conducted by De Haart et al. [13], also pointed out that the increasing conversion rate increases degradation even though not significantly if it is within the range of 8-75%.

A further examination of the data reveals what the model has learned from the data. The data collected shows that the degradation rate is higher at the beginning of the experiments. Experimental studies have shown that at the beginning of stack experiments, there is an initial drop in cell voltage, leading to a pronounced degradation at the beginning of the experiment [15]. Fang et al. [54] observed that degradation rates were neither constant nor linear, and it was usually higher at the beginning of the test experiment. Therefore, the model has learned from the data that the degradation rate is higher at the beginning of the experiment, whereas in most stack tests, a smaller conversion rate is used at the beginning.

Further, increasing the conversion rate later in the test does not lead to pronounced degradation phenomena, which is usually observed at the beginning of the performance test. Another contributory factor that results in this seemingly contradictory phenomenon is that, given the same operating conditions, fuel utilisation and temperature, the degradation rate at the experiment's beginning is higher than at any other time throughout the test. It becomes necessary to account for SOC's pronounced degradation behaviour at the stack test's beginning. The cumulative charge transfer over the load phases normalised the account for this voltage and resistance degradation rate. This was achieved by multiplying the voltage and degradation

rate by the normalising charge. The result of this regression analysis is presented in Figures 13 and 14.

1.3 Regression Analysis With Normal Priors Using Charge Normalised Voltage And Resistance Degradation Rate As The Regressand

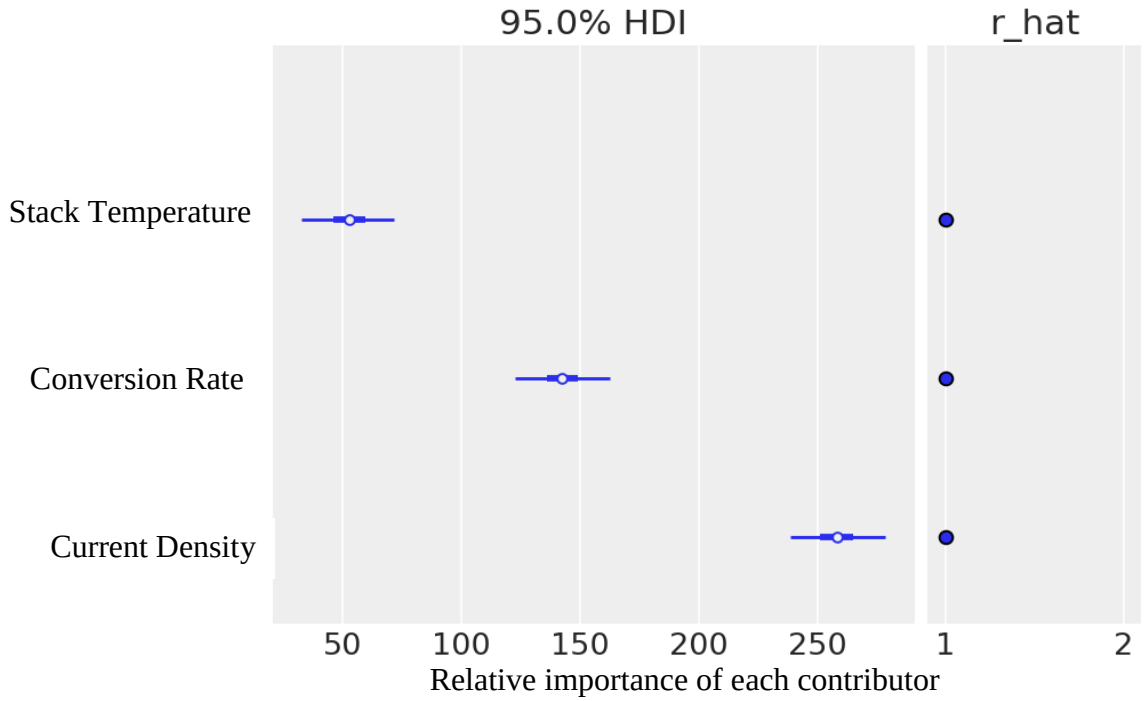

Figure 13: *Posterior Distribution of Predictor Coefficient with Normalised Voltage Degradation Rate as the Regressand*

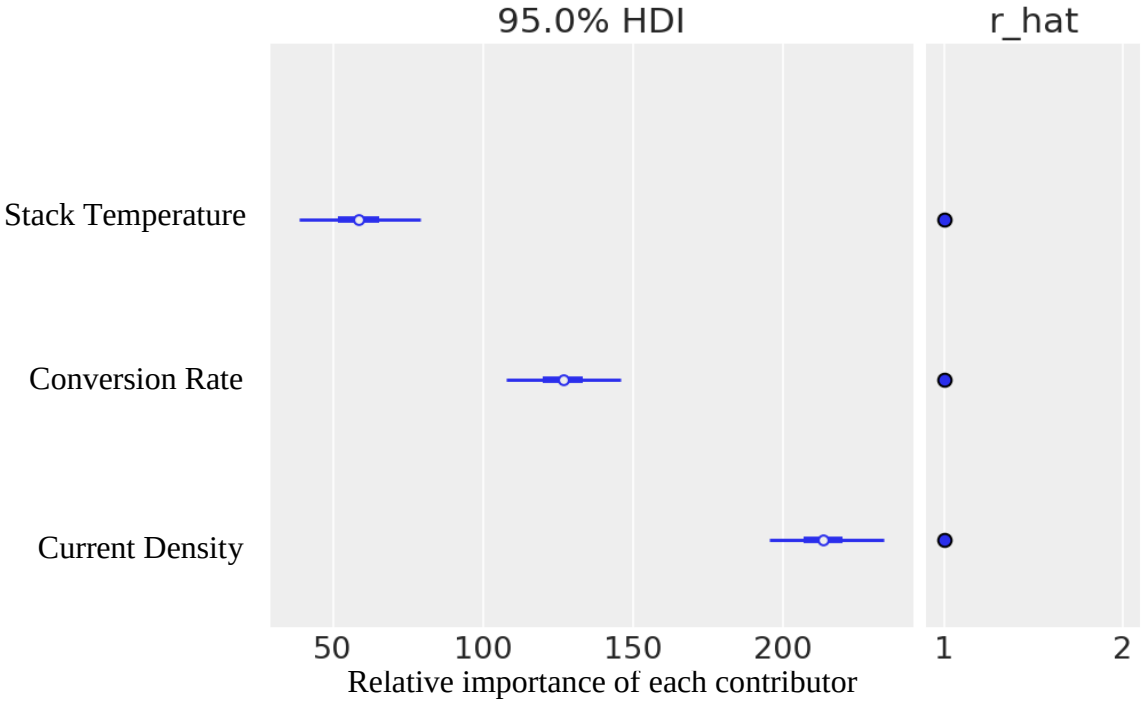

Figure 14:*Posterior Distribution of Predictor Coefficient with Normalized Resistance Degradation Rate as the Regressand*

Regression analysis for charge normalised voltage and resistance degradation rate as the regressand is shown in Figure 13 and Figure 14, respectively. The Highest Density Interval of the posterior distribution of the coefficients of the regressors shows the main contributor to SOC degradation. As observed previously, the current density is the most contributing factor to the SOC degradation rate. Operating at higher density will result in worse degradation, that is, a higher degradation rate. Conversion rate is the second leading contributing factor leading to SOC degradation. After normalising both the voltage and resistance degradation rate with charge transfer, the degradation rate increases with increasing conversion rate. The result after normalisation is consistent with De Haart et al.'s [13] findings. Mogensen et al. [55] stated that cell degradation and degradation rate mainly depend on current density, as described in the literature.

CONCLUSION

An investigation of the main contributors in SOC degradation by multivariate regression has been conducted to identify the individual influence of operating parameters: current density, conversion rate and stack density. From the analysis conducted in this study using Bayesian inference, the current density is the main contributor to SOC degradation, while the conversion rate is the second leading factor to SOC degradation. This finding agrees with what was previously reported in the literature.

GENERAL CONCLUSION AND PERSPECTIVE

GENERAL CONCLUSION AND PERSPECTIVE

General conclusion

Solid oxide cell is a promising technology expected to play a crucial role in energy transition and decarbonisation goal. Durability and degradation impact its commercialisation. In this study, the influence of individual operating conditions on SOC degradation has been investigated. Experimental data from different stack experiments having homogenous material properties and configurations were used for analysis in this study. In order to quantify the influence of operating parameters on SOC degradation rate, the different load operations for fuel and electrolysis operations were identified, and the degradation rate for each identified phase was estimated. Each load operation's degradation rate and corresponding operation conditions, such as current density, stack temperature and utilisation rate, were collected and tabulated. Using Bayesian multivariate regression analysis to investigate the relationship between the dependent variable (degradation rate) and independent variable (the operating conditions: current density, utilisation rate and stack temperature). The analysis in this study reveals that current density is the main contributor to SOC degradation while conversion rate is the second leading contributor.

General Perspective

This research agrees with previous findings and has contributed to our understanding of which operation conditions significantly contribute to Solid Oxide Cell degradation. However, the scope of this research is still very limited. The operating conditions investigated in this study did not encompass all practical operating conditions. Further research should be done to investigate other operating parameters, such as air utilisation, gas composition thermocycling, and emergency shutdown. Further study can consider operational incidents such as thermal cycles and emergency shutdowns on SOC degradation. Degradation rate measurement is not linear and varies with time. As pointed out in this work, the degradation rate is higher at the beginning of the stack experiment until it becomes pseudo-linear after a certain time. Further study can be done employing a different normalisation approach, taking into the variation of degradation rate with time.

References

[1] Li, M., Wu, J., Chen, Z., Dong, J., Peng, Z., Xiong, K., Rao, M., Chen, C., & Li, X. (2022). Data-Driven Voltage Prognostic for Solid Oxide Fuel Cell System Based on Deep Learning. *Energies*, *15*(17). https://doi.org/10.3390/en15176294

[2] Königshofer, B., Höber, M., Nusev, G., Boškoski, P., Hochenauer, C., & Subotić, V. (2022). Accelerated degradation for solid oxide electrolysers: Analysis and prediction of performance for varying operating environments. *Journal of Power Sources*, *523*. https://doi.org/10.1016/j.jpowsour.2022.230982

[3] Biswas, S., Rathore, S. S., Kulkarni, A. P., Giddey, S., & Bhattacharya, S. (2021). A theoretical study on reversible solid oxide cells as key enablers of cyclic conversion between electrical energy and fuel. *Energies*, *14*(15). https://doi.org/10.3390/en14154517.

[4] S. Biswas, S. S. Rathore, A. P. Kulkarni, S. Giddey, and S. Bhattacharya, "A theoretical study on reversible solid oxide cells as key enablers of cyclic conversion between electrical energy and fuel," *Energies (Basel)*, vol. 14, no. 15, Aug. 2021, doi: 10.3390/en14154517.

[5] Venkataraman, V., Pérez-Fortes, M., Wang, L., Hajimolana, Y. S., Boigues-Muñoz, C., Agostini, A., McPhail, S. J., Maréchal, F., van Herle, J., & Aravind, P. v. (2019). Reversible solid oxide systems for energy and chemical applications – Review & perspectives. In *Journal of Energy Storage* (Vol. 24). Elsevier Ltd. https://doi.org/10.1016/j.est.2019.100782

[6] del Pozo Gonzalez, H., Torrell, M., Bernadet, L., Bianchi, F. D., Trilla, L., Tarancón, A., & Domínguez-García, J. L. (2023). Mathematical Modeling and Thermal Control of a 1.5 kW Reversible Solid Oxide Stack for 24/7 Hydrogen Plants. *Mathematics*, *11*(2), 1–18. https://doi.org/10.3390/math11020366.

[7] Subotić, V., & Hochenauer, C. (2022). Analysis of solid oxide fuel and electrolysis cells operated in a real-system environment: State-of-the-health diagnostic, failure modes, degradation mitigation and performance regeneration. *Progress in Energy and Combustion Science*, *93*(August). https://doi.org/10.1016/j.pecs.2022.101011.

[8] Wu, J., Myung, J., Ding, D., & Zhu, T. (2021). *Editorial : High Temperature Solid Oxide Cells*. *9*(September), 1–3. https://doi.org/10.3389/fchem.2021.719826

[9] Wendel, C. H., Kazempoor, P., & Braun, R. J. (2016). A thermodynamic approach for selecting operating conditions in the design of reversible solid oxide cell energy systems. *Journal of Power Sources*, *301*, 93–104. https://doi.org/10.1016/j.jpowsour.2015.09.093.

[10] McPhail, S. J., Frangini, S., Laurencin, J., Effori, E., Abaza, A., Padinjarethil, A. K., Hagen, A., Léon, A., Brisse, A., Vladikova, D., Burdin, B., Bianchi, F. R., Bosio, B., Piccardo, P., Spotorno, R., Uchida, H., Polverino, P., Adinolfi, E. A., Postiglione, F., … Van herle, J. (2022). Addressing planar solid oxide cell degradation mechanisms: A

critical review of selected components. In *Electrochemical Science Advances* (Vol. 2, Issue 5). John Wiley and Sons Inc. https://doi.org/10.1002/elsa.202100024.

[11] Hagen, A., Barfod, R., Hendriksen, P. V., Liu, Y.-L., & Ramousse, S. (2006). Degradation of Anode Supported SOFCs as a Function of Temperature and Current Load. *Journal of The Electrochemical Society*, *153*(6), A1165. https://doi.org/10.1149/1.2193400.

[12] Koch, S., Hendriksen, P. V., MMogensen, Liu, Y. L., Dekker, N., Rietveld, B., De Haart, B., & Tietz, F. (2006). Solid oxide fuel cell performance under severe operating conditions. *Fuel Cells*, *6*(2), 130–136. https://doi.org/10.1002/fuce.200500112.

[13] De Haart, L. G. J., Mougin, J., Posdziech, O., Kiviaho, J., & Menzler, N. H. (2009). Stack degradation in dependence of operation parameters; the real-SOFC sensitivity analysis. *Fuel Cells*, *9*(6), 794–804. https://doi.org/10.1002/fuce.200800146.

[14] Fang, Q., de Haart, U., Schäfer, D., Thaler, F., Rangel-Hernandez, V., Peters, R., & Blum, L. (2020). Degradation Analysis of an SOFC Short Stack Subject to 10,000 h of Operation. *Journal of The Electrochemical Society*, *167*(14), 144508. https://doi.org/10.1149/1945-7111/abc843.

[15] Yang, X., Du, Z., Zhang, Q., Lyu, Z., Liu, S., Liu, Z., Han, M., & Zhao, H. (2023). Effects of operating conditions on the performance degradation and anode microstructure evolution of anode-supported solid oxide fuel cells. *International Journal of Minerals, Metallurgy and Materials*, *30*(6), 1181–1189. https://doi.org/10.1007/s12613-023-2616-7**.**

[16] Skafte, T. L. (2017). Lifetime limiting effects in pre-commercial solid oxide cell devices. In *Ph.d. thesis*

[17] Cooper, S. J., & Brandon, N. P. (2017). An Introduction to Solid Oxide Fuel Cell Materials, Technology and Applications. In *Solid Oxide Fuel Cell Lifetime and Reliability: Critical Challenges in Fuel Cells* (pp. 1–18). Elsevier Inc. https://doi.org/10.1016/B978-0-08-101102-7.00001-5

[18] He, S., Zou, Y., Chen, K., & Jiang, S. P. (2023). A critical review of key materials and issues in solid oxide cells. *Interdisciplinary Materials*, *2*(1), 111–136. https://doi.org/10.1002/idm2.12068

[19] Dewa, M., Elharati, M. A., Mohammed Hussain, A., Wu, D., Grant Norton, M., Ha, S., Authors, C., & Ha suha, S. (2022). *Metal-Supported Solid Oxide Fuel Cell System with Infiltrated Reforming Catalyst Layer Operating under Direct Ethanol Feed Configuration*.

[20] Peng, J., Zhao, D., Xu, Y., Wu, X., & Li, X. (2023). Comprehensive Analysis of Solid Oxide Fuel Cell Performance Degradation Mechanism, Prediction, and Optimization Studies. In *Energies* (Vol. 16, Issue 2). MDPI. https://doi.org/10.3390/en16020788.

[21] Störmer Heike. (2022, September 30). *Solid Oxide Fuel Cells (SOFC) and (SOEC)*. Laboratory for Electron Microscopy, Karlsruhe Institute of Technology.

[22] Chen, K., & Jiang, S. P. (2016). Review—Materials Degradation of Solid Oxide Electrolysis Cells. *Journal of The Electrochemical Society*, *163*(11), F3070–F3083. https://doi.org/10.1149/2.0101611jes.

[23] Løye, T. (2023). General rights Lifetime limiting effects in pre-commercial solid oxide cell devices. In *Downloaded from orbit.dtu.dk on*.

[24] Hauch, A., Küngas, R., Blennow, P., Hansen, A. B., Hansen, J. B., Mathiesen, B. V., & Mogensen, M. B. (2020). Recent advances in solid oxide cell technology for electrolysis. *Science*, *370*(6513). https://doi.org/10.1126/science.aba6118.

[25] "Fuel Cell Handbook (Seventh Edition)," 2004.

[26] Gasik, M., & Institute of Materials, M. (2008). *Materials for fuel cells*. CRC Press.

[27] Mänken, C. F. (2020). *Modelling and implementation of a reversible solid oxide cell (rSOC) in an open gas turbine cycle*.

[28] Khotseng, L. (2020). Fuel Cell Thermodynamics. In *Thermodynamics and Energy Engineering*. IntechOpen. https://doi.org/10.5772/intechopen.90141.

[29] Zarabi Golkhatmi, S., Asghar, M. I., & Lund, P. D. (2022). A review on solid oxide fuel cell durability: Latest progress, mechanisms, and study tools. *Renewable and Sustainable Energy Reviews*, *161*(February), 112339. https://doi.org/10.1016/j.rser.2022.112339.

[30] Hsieh, Y. D., Chan, Y. H., & Shy, S. S. (2015). Effects of pressurization and temperature on power generating characteristics and impedances of anode-supported and electrolyte-supported planar solid oxide fuel cells. *Journal of Power Sources*, *299*, 1–10. https://doi.org/10.1016/j.jpowsour.2015.08.080.

[31] Buccheri, M. A., Singh, A., & Hill, J. M. (2011). Anode- versus electrolyte-supported Ni-YSZ/YSZ/Pt SOFCs: Effect of cell design on OCV, performance and carbon formation for the direct utilization of dry methane. *Journal of Power Sources*, *196*(3), 968–976. https://doi.org/10.1016/j.jpowsour.2010.08.073.

[32] Park, B. K., Lee, J. W., Lee, S. B., Lim, T. H., Park, S. J., Song, R. H., & Shin, D. R. (2012). A flat-tubular solid oxide fuel cell with a dense interconnect film coated on the porous anode support. *Journal of Power Sources*, *213*, 218–222. https://doi.org/10.1016/j.jpowsour.2012.04.025.

[33] Yan, Y. (2018). *Degradation Study of SOC Stacks with Impedance Spectroscopy*.

[34] Cassidy, M., Neagu, D., Savaniu, C., & Boldrin, P. (2017). New Materials for Improved Durability and Robustness in Solid Oxide Fuel Cell. In *Solid Oxide Fuel Cell Lifetime and Reliability: Critical Challenges in Fuel Cells* (pp. 193–216). Elsevier Inc. https://doi.org/10.1016/B978-0-08-101102-7.00010-6.

[35] Blum, L., & Riensche, E. (2009). Fuel Cells - Solid Oxide Fuel Cells | Systems. *Encyclopedia of Electrochemical Power Sources*, 99–119. https://doi.org/10.1016/B978-044452745-5.00262-8.

[36] Dwivedi, S. (2020). Solid oxide fuel cell: Materials for anode, cathode and electrolyte. *International Journal of Hydrogen Energy*, *45*(44), 23988–24013. https://doi.org/10.1016/j.ijhydene.2019.11.234.

[37] Tariq, F., Ruiz-Trejo, E., Bertei, A., Boldrin, P., & Brandon, N. P. (2017). Microstructural Degradation: Mechanisms, Quantification, Modeling and Design Strategies to Enhance the Durability of Solid Oxide Fuel Cell Electrodes. In *Solid Oxide Fuel Cell Lifetime and Reliability: Critical Challenges in Fuel Cells* (pp. 79–99). Elsevier Inc. https://doi.org/10.1016/B978-0-08-101102-7.00005-2.

[38] Gómez, S. Y., & Hotza, D. (2016). Current developments in reversible solid oxide fuel cells. In *Renewable and Sustainable Energy Reviews* (Vol. 61, pp. 155–174). Elsevier Ltd. https://doi.org/10.1016/j.rser.2016.03.005.

[39] Aphale, A., Liang, C., Hu, B., & Singh, P. (2017). Cathode Degradation From Airborne Contaminants in Solid Oxide Fuel Cells: A Review. In *Solid Oxide Fuel Cell Lifetime and Reliability: Critical Challenges in Fuel Cells* (pp. 101–119). Elsevier Inc. https://doi.org/10.1016/B978-0-08-101102-7.00006-4.

[40] Jiang, S. P. (2016). Challenges in the development of reversible solid oxide cell technologies: A mini review. In *Asia-Pacific Journal of Chemical Engineering* (Vol. 11, Issue 3, pp. 386–391). John Wiley and Sons Ltd. https://doi.org/10.1002/apj.1987.

[41] Sreedhar, I., Agarwal, B., Goyal, P., & Agarwal, A. (2020). An overview of degradation in solid oxide fuel cells-potential clean power sources. In *Journal of Solid State Electrochemistry* (Vol. 24, Issue 6, pp. 1239–1270). Springer. https://doi.org/10.1007/s10008-020-04584-4.

[42] Gunawan, G., Sulistyo, S., & Setyawan, I. (2021). Progress in Glass-Ceramic Seal for Solid Oxide Fuel Cell. *Journal of Advanced Research in Fluid Mechanics and Thermal Sciences, 82*(1), 39–50. https://doi.org/10.37934/arfmts.82.1.3950.

[43] Fergus, J. W. (2005). Sealants for solid oxide fuel cells. In *Journal of Power Sources* (Vol. 147, Issues 1–2, pp. 46–57). https://doi.org/10.1016/j.jpowsour.2005.05.002.

[44] Knibbe, R., Hauch, A., Hjelm, J., Ebbesen, S. D., & Mogensen, M. (2011). Durability of solid oxide cells. *Green, 1*(2), 141–169. https://doi.org/10.1515/GREEN.2011.015.

[45] Chen, K., & Jiang, S. P. (2020). Surface Segregation in Solid Oxide Cell Oxygen Electrodes: Phenomena, Mitigation Strategies and Electrochemical Properties. In *Electrochemical Energy Reviews* (Vol. 3, Issue 4, pp. 730–765). Springer Science and Business Media B.V. https://doi.org/10.1007/s41918-020-00078-z.

[46] Moçoteguy, P., & Brisse, A. (2013). A review and comprehensive analysis of degradation mechanisms of solid oxide electrolysis cells. In *International Journal of Hydrogen Energy* (Vol. 38, Issue 36, pp. 15887–15902). https://doi.org/10.1016/j.ijhydene.2013.09.045.

[47] Kim, B. K., Kim, D. I., & Yi, K. W. (2018). Suppression of Cr evaporation by Co electroplating and underlying Cr retention mechanisms for the 22 wt.% Cr containing ferritic stainless steel. *Corrosion Science*, *130*, 45–55. https://doi.org/10.1016/j.corsci.2017.10.019.

[48] Subotić, V., Thaller, T., Königshofer, B., Menzler, N. H., Bucher, E., Egger, A., & Hochenauer, C. (2020). Performance assessment of industrial-sized solid oxide cells operated in a reversible mode: Detailed numerical and experimental study. *International Journal of Hydrogen Energy*, *45*(53), 29166–29185. https://doi.org/10.1016/j.ijhydene.2020.07.165.

[49] James, G., Witten, D., Hastie, T., & Tibshirani, R. (2013). *Springer Texts in Statistics An Introduction to Statistical Learning*. http://www.springer.com/series/417

[50] Martin, O. (2018). *Bayesian analysis with Python : introduction to statistical modeling and probabilistic programming using PyMC3 and ArviZ*.

[51] Koehrsen Will. (2018, April 14). *Introduction to Bayesian Linear Regression*. Towards Data Science.

[52] Van de Schoot, R., Kaplan, D., Denissen, J., Asendorpf, J. B., Neyer, F. J., & van Aken, M. A. G. (2014). A Gentle Introduction to Bayesian Analysis: Applications to Developmental Research. *Child Development*, *85*(3), 842–860. https://doi.org/10.1111/cdev.12169.

[53] Salvatier, J., Wiecki, T. V., & Fonnesbeck, C. (2016). Probabilistic programming in Python using PyMC3. *PeerJ Computer Science*, *2016*(4). https://doi.org/10.7717/peerj-cs.55.

[54] Fang, Q., Blum, L., & Stolten, D. (2019). Electrochemical Performance and Degradation Analysis of an SOFC Short Stack Following Operation of More than 100,000 Hours. *Journal of The Electrochemical Society*, *166*(16), F1320–F1325. https://doi.org/10.1149/2.0751916jes.

[55] Mogensen, M. B., Chen, M., Frandsen, H. L., Graves, C., Hansen, J. B., Hansen, K. V., Hauch, A., Jacobsen, T., Jensen, S. H., Skafte, T. L., & Sun, X. (2019). Reversible solid-oxide cells for clean and sustainable energy. In *Clean Energy* (Vol. 3, Issue 3, pp. 175–201). Oxford University Press. https://doi.org/10.1093/ce/zkz023.

APPENDIX

A1: Load Operation and Corresponding Operating Parameters for the analysed Stack Experiments

Experiment	SK672_F1004_102											
Phases	1	2	3	4	5	6	7	8	9	10	11	12
Current density	0.498326	0.497829	0.497838	0.497842	0.5	0.747216	0.747424	0.995934	0.996273	0.996303	0.995709	0.996428
Fuel utilization	39.86609	59.95356	59.95465	74.8433	80.57554	80.08437	80.10667	79.67473	79.70181	79.70427	79.65672	79.71427
Steam utilization												
Stack temperature	726.2444	724.9027	724.9216	726.0341	725.5	726.5602	726.5739	731.8342	732.7	733.8864	734.358	739.0381
Mean Voltage Cell_1	0.900263	0.874255	0.873588	0.855004	0.845099	0.790171	0.788428	0.723043	0.708616	0.694367	0.685977	0.644234
Mean Voltage Cell_2	0.906386	0.879248	0.878666	0.858103	0.847316	0.798188	0.796972	0.740587	0.731575	0.72331	0.718891	0.704803
Mean Voltage Cell_3	0.904127	0.876235	0.875623	0.853492	0.841128	0.791393	0.789981	0.732583	0.723392	0.71453	0.709752	0.694772
Mean Voltage Cell_4	0.900411	0.872091	0.871971	0.849237	0.836049	0.785952	0.784576	0.725243	0.71649	0.707725	0.703491	0.689667
Degradation Rate Cell_1	-0.00323	-0.0151	0.00521	-0.00329	-0.00221	-0.00587	-0.00324	-0.00757	-0.00796	-0.00635	-0.0094	-0.05264
Degradation Rate Cell_2	-0.00241	-0.01262	0.00531	-0.00315	-0.00195	-0.00489	-0.00238	-0.00502	-0.00497	-0.00293	-0.0053	-0.03394
Degradation Rate Cell_3	-0.00248	-0.01238	0.004831	-0.00396	-0.00231	-0.00475	-0.00207	-0.00497	-0.00521	-0.00327	-0.00565	-0.03436
Degradation Rate Cell_4	-0.00144	-0.00205	0.005123	-0.00338	-0.0031	-0.00639	-0.00465	-0.00405	-0.00507	-0.00272	-0.00462	-0.03507
Operating Time	60	4	7	32	51	51	9	82	99	32	55	25
Operating Time (h)	1431	93	161	767	1216	1216	217	1977	2367	757	1329	604
Charge Transfer	2.05E+08	13345768	23143458	1.1E+08	1.75E+08	2.62E+08	46800660	5.67E+08	6.79E+08	2.17E+08	3.81E+08	1.74E+08
C_Charge Transfer	2.05E+08	2.19E+08	2.42E+08	3.52E+08	5.27E+08	7.89E+08	8.36E+08	1.4E+09	2.08E+09	2.3E+09	2.68E+09	2.85E+09
Number of Layer	4	4	4	4	4	4	4	4	4	4	4	4

Experiment	SK706_F1004_111									
Phases	1	2	3	4	5	6	7	8	9	10
Current density	0.500077	0.500256	0.500298	0.500231	0.500278	0.500297	0.500372	1.000399	1.000414	1.00047
Fuel utilization	40.06957	40.07084	40.0731	40.04879	40.11526	40.06141	40.0734	40.11659	40.03663	20.48475
Steam utilization										
Stack temperature	708.5896	705.9839	706.1764	708.1108	707.358	707.9215	707.2783	702.8675	694.4201	701.0898
Mean Voltage Cell_1	0.905161	0.893215	0.88831	0.888125	0.883297	0.882557	0.881038	0.770155	0.756692	0.76044
Mean Voltage Cell_2	0.888534	0.885403	0.880867	0.879861	0.875319	0.874988	0.873429	0.753186	0.739392	0.745402
Mean Voltage Cell_3	0.912625	0.906282	0.901957	0.900018	0.894746	0.893921	0.892291	0.790838	0.777414	0.773457
Mean Voltage Cell_4	0.889705	0.886003	0.881178	0.879899	0.87502	0.874517	0.87287	0.745198	0.73162	0.73599
Degradation Rate Cel	-0.00593	-0.02012	-0.00115	-0.00765	-0.0018	-0.01308	-0.00562	-0.12012	-0.08196	-0.01164
Degradation Rate Cel	-0.00178	-0.00598	-0.00463	-0.00833	-0.00039	-0.01377	-0.00711	-0.13562	-0.08753	-0.01159
Degradation Rate Cel	0.000959	-0.00549	-0.00502	-0.00851	-0.00157	-0.01364	-0.00735	-0.10972	-0.06539	-0.01039
Degradation Rate Cel	-0.00283	-0.00661	-0.00516	-0.00891	-0.00105	-0.0145	-0.00798	-0.14373	-0.07628	-0.01311
Operating Time	14	21	21	7	9	6	4	8	6	11
Operating Time (h)	325	503	501	162	222	145	97	180	140	270
Charge Transfer	46927261	72476298	72211036	23403611	32050626	20976470	14089471	52016736	40538380	77892616
C_Charge Transfer	46927261	1.19E+08	1.92E+08	2.15E+08	2.47E+08	2.68E+08	2.82E+08	3.34E+08	3.75E+08	4.53E+08
Number of Layer	4	4	4	4	4	4	4	4	4	4

Experiment	SK708_F1002_197			
Phases	1	2	3	4
Current density	-0.50012	-0.50012	-0.50012	-0.50008
Fuel utilization				
Steam utilization	49.78858	49.78858	49.78857	49.78451
Stack temperature	747.8358	747.7516	746.9822	747.8375
Mean Voltage Cell_1	1.099978	1.148174	1.12572	1.154531
Mean Voltage Cell_2	1.094684	1.139378	1.118111	1.140141
Degradation Rate Cell_	0.016475	0.111504	0.024459	0.055146
Degradation Rate Cell_	0.016764	0.085789	0.027344	0.033156
Operating Time	13	2	2	20
Operating Time (h)	305	38	46	473
Charge Transfer	44027008	5554987	6712082	68159459
C_Charge Transfer	44027008	49581995	56294077	1.24E+08
Number of Layer	2	2	2	2

Experiment	SK709_F1005_15
Phases	1
Current density	0.500028481
Fuel utilization	40.00227845
Steam utilization	
Stack temperature	702.947895
Mean Voltage Cell_1	0.910436643
Mean Voltage Cell_2	0.910009132
Mean Voltage Cell_3	0.917902969
Mean Voltage Cell_4	0.913760089
Mean Voltage Cell_5	0.915437364
Degradation Rate Cell_1	0.009214076
Degradation Rate Cell_2	0.007351185
Degradation Rate Cell_3	0.009207866
Degradation Rate Cell_4	0.008167367
Degradation Rate Cell_5	0.007394462
Operating Time	7
Operating Time (h)	168
Charge Transfer	24253406.98
C_Charge Transfer	24253406.98
Number of Layer	5

Experiment	SK713_F1004_123		
Phases	1	2	3
Current density	0.49857	0.496956	0.497036
Fuel utilization	39.88563	39.75646	39.76288
Steam utilization			
Stack temperature	724.3349	722.0542	722.0269
Mean Voltage Cell_1	0.906019	0.851653	0.855825
Mean Voltage Cell_2	0.913706	0.874664	0.874787
Mean Voltage Cell_3	0.909214	0.872023	0.87172
Mean Voltage Cell_4	0.907939	0.864789	0.864901
Degradation Rate Cell_1	-0.00837	0.010585	0.011388
Degradation Rate Cell_2	-0.00709	-0.00468	-0.00013
Degradation Rate Cell_3	-0.00725	-0.00638	-0.00301
Degradation Rate Cell_4	-0.00684	-0.00541	0.000451
Operating Time	34	7	12
Operating Time (h)	813	174	289
Charge Transfer	1.17E+08	24934430	41402701
C_Charge Transfer	1.17E+08	1.42E+08	1.83E+08
Number of Layer	4	4	4

Experiment	SK714_F1004_110					
Phases	1	2	3	4	5	6
Current density	-1.44994	-1.44996	-1.44996	-1.125	-1.125	-1.125
Fuel utilization						
Steam utilization	79.82195	79.82308	79.82327	80.63735	80.63735	80.63735
Stack temperature	759.8701	759.7859	761.7082	758.376	760.2455	761.2075
Mean Voltage Cell_1	1.310673	1.324164	1.329895	1.27677	1.295693	1.307177
Mean Voltage Cell_2	1.276851	1.293539	1.301878	1.269262	1.292154	1.308408
Mean Voltage Cell_3	1.282038	1.297738	1.304839	1.265206	1.284151	1.297134
Mean Voltage Cell_4	1.284861	1.300817	1.309157	1.267883	1.301477	1.311396
Degradation Rate Cell_1	0.118746	-0.00628	0.066918	0.038407	0.031097	0.023795
Degradation Rate Cell_2	0.127232	-0.00075	0.097396	0.048377	0.045403	0.033252
Degradation Rate Cell_3	0.110216	0.01733	0.0802	0.03887	0.03942	0.024756
Degradation Rate Cell_4	0.135414	0.079416	0.08827	0.044284	0.033005	0.014578
Operating Time	2	1	6	7	17	18
Operating Time (h)	52	22	141	168	400	427
Charge Transfer	21818674	9374849	59061095	54680430	1.3E+08	1.38E+08
C_Charge Transfer	21818674	31193523	90254618	1.45E+08	2.75E+08	4.13E+08
Number of Layer	4	4	4	4	4	4

Experiment	SK729_F1004_124							
Phases	1	2	3	4	5	6	7	8
Current density	0.500204	0.500187	-0.60012	-0.65012	-0.65012	-0.70012	-0.69924	-0.70012
Fuel utilization	40.05498	40.05155						
Steam utilization			73.32193	79.43083	79.43083	80.07973	79.97882	80.07972
Stack temperature	723.6239	724.0109	718.9215	721.9835	722.2237	724.157	724.5833	721.9696
Mean Voltage Cell_1	0.905698	0.897874	1.230095	1.267973	1.26358	1.290276	1.293047	1.235071
Mean Voltage Cell_2	0.910035	0.902378	1.213575	1.249146	1.247657	1.27205	1.277427	1.22787
Mean Voltage Cell_3	0.904408	0.896137	1.216673	1.25262	1.251888	1.276333	1.279606	1.229958
Mean Voltage Cell_4	0.899399	0.889767	1.244766	1.290787	1.288707	1.318533	1.31796	1.25109
Degradation Rate Cell_1	-0.00414	-0.00622	0.033436	-0.05218	-0.00431	-0.02125	0.016743	0.023076
Degradation Rate Cell_2	-0.00527	-0.00575	0.033465	-0.01943	0.003986	-0.01292	0.02117	0.01804
Degradation Rate Cell_3	-0.0047	-0.00652	0.033977	-0.01422	0.008872	-0.01126	0.025246	0.019627
Degradation Rate Cell_4	-0.01163	-0.00563	0.036713	-0.0341	0.003502	-0.01518	0.007388	0.014626
Operating Time	22	53	7	7	8	6	7	21
Operating Time (h)	522	1263	159	177	186	150	176	503
Charge Transfer	75251507	1.82E+08	27532767	33190700	34938241	30379822	35459997	1.02E+08
C_Charge Transfer	75251507	2.57E+08	2.85E+08	3.18E+08	3.53E+08	3.83E+08	4.19E+08	5.2E+08
Number of Layer	4	4	4	4	4	4	4	4

Experiment	SK730_F1004_115				
Phases	1	2	3	4	5
Current density	0.500092	0.500175	-0.70012	-0.70012	-0.70012
Fuel utilization	40.09523	40.09541			
Steam utilization			80.07974	80.07974	80.07974
Stack temperature	712.6868	712.0172	798.6774	797.9268	797.8709
Mean Voltage Cell_1	0.869218	0.865697	1.14358	1.085955	1.088745
Mean Voltage Cell_2	0.87192	0.867648	1.149207	1.091297	1.094468
Mean Voltage Cell_3	0.852067	0.847004	1.165748	1.09412	1.097534
Mean Voltage Cell_4	0.870234	0.866689	1.143927	1.08882	1.091786
Degradation Rate Cell_1	-0.00704	-0.00507	0.015296	0.022616	0.009391
Degradation Rate Cell_2	-0.00686	-0.00572	0.01917	0.027284	0.008401
Degradation Rate Cell_3	-0.00896	-0.00602	0.001264	0.030643	0.011686
Degradation Rate Cell_4	-0.00637	-0.00566	0.020864	0.021894	0.008026
Operating Time	28	22	42	5	10
Operating Time (h)	666	531	1003	128	236
Charge Transfer	96023691	76576721	2.02E+08	25987551	47660052
C_Charge Transfer	96023691	1.73E+08	3.75E+08	4.01E+08	4.49E+08
Number of Layer	4	4	4	4	4

Experiment	SK736_F1005_17		
Phases	1	2	3
Current density	0.499329	0.499351	0.499354
Fuel utilization	39.79245	59.89765	79.96825
Steam utilization			
Stack temperature	711.82	710.9407	710.0513
Mean Voltage Cell_1	0.877874	0.852557	0.804197
Mean Voltage Cell_2	0.899558	0.872282	0.841027
Mean Voltage Cell_3	0.912747	0.885636	0.855359
Mean Voltage Cell_4	0.900122	0.872524	0.841147
Mean Voltage Cell_5	0.906963	0.880145	0.851445
Degradation Rate Cell_1	-0.01686	-0.01012	-0.01948
Degradation Rate Cell_2	-0.00599	-0.00279	-0.00376
Degradation Rate Cell_3	-0.00471	-0.00237	-0.00356
Degradation Rate Cell_4	-0.00547	-0.00254	-0.00344
Degradation Rate Cell_5	-0.00521	-0.00277	-0.0037
Operating Time	51	42	21
Operating Time (h)	1224	1007	498
Charge Transfer	1.76E+08	1.45E+08	71726471
C_Charge Transfer	1.76E+08	3.21E+08	3.93E+08
Number of Layer	5	5	5

Experiment	SK738_F1004_122	
Phases	1	2
Current density	0.497733	0.497751
Fuel utilization	39.81865	39.81865
Steam utilization		
Stack temperature	727.024	727.3986
Mean Voltage Cell_1	0.920786	0.91937
Mean Voltage Cell_2	0.926772	0.926004
Mean Voltage Cell_3	0.921125	0.920359
Mean Voltage Cell_4	0.927533	0.926769
Degradation Rate Cell_1	-0.01308	-0.00414
Degradation Rate Cell_2	-0.01166	-0.00129
Degradation Rate Cell_3	-0.01208	-0.00049
Degradation Rate Cell_4	-0.01193	-0.00058
Operating Time	7	14
Operating Time (h)	164	330
Charge Transfer	23639029	47419598
C_Charge Transfer	23639029	71058626
Number of Layer	4	4

Experiment	SK741_F1004_132						
Phases	1	2	3	4	5	6	7
Current density	0.74761	0.747642	0.747656	0.747632	0.747651	0.747667	0.747698
Fuel utilization	39.87251	39.87423	39.87499	39.87373	39.87471	39.87558	39.87725
Steam utilization							
Stack temperature	792.7596	793.5042	793.82	794.0719	794.3092	794.5596	795.1306
Mean Voltage Cell_1	0.726528	0.726274	0.725731	0.72489	0.72395	0.722577	0.718776
Mean Voltage Cell_2	0.733041	0.720481	0.716218	0.71152	0.707422	0.702026	0.69132
Mean Voltage Cell_3	0.738733	0.72625	0.721677	0.716474	0.711753	0.705305	0.691785
Mean Voltage Cell_4	0.715104	0.685808	0.674608	0.662918	0.652971	0.640554	0.618388
Degradation Rate Cell_1	-0.00104	-0.00266	-0.01103	-0.00651	-0.00857	-0.00923	-0.00755
Degradation Rate Cell_2	-0.08097	-0.03856	-0.04755	-0.03568	-0.04085	-0.03231	-0.03087
Degradation Rate Cell_3	-0.07648	-0.03938	-0.0522	-0.04025	-0.04806	-0.03863	-0.04202
Degradation Rate Cell_4	-0.17417	-0.09331	-0.10524	-0.08378	-0.0972	-0.06863	-0.06964
Operating Time	12	6	7	8	6	13	18
Operating Time (h)	285	155	156	185	135	301	443
Charge Transfer	61507584	33518276	33716294	40048771	29176327	64939171	95555860
C_Charge Transfer	61507584	95025860	1.29E+08	1.69E+08	1.98E+08	2.63E+08	3.58E+08
Number of Layer	4	4	4	4	4	4	4

Experiment	SK755_F1002_198					
Phases	1	2	3	4	5	6
Current density	-0.50012	-0.50012	-0.50012	-0.50012	-0.50012	-1.00013
Fuel utilization						
Steam utilization	49.78857	49.78858	49.78858	49.78858	25.01008	50.0139
Stack temperature	698.9305	698.6778	699.3475	698.9047	696.1416	699.8344
Mean Voltage Cell_1	1.185806	1.189298	1.194583	1.197237	1.10395	1.373276
Mean Voltage Cell_2	1.170699	1.173989	1.180411	1.184158	1.098858	1.365
Degradation Rate Cell_1	0.030156	0.013176	0.015517	0.011478	0.011478	0.037472
Degradation Rate Cell_2	0.024984	0.015039	0.018518	0.012433	0.012433	0.039325
Operating Time	8	6	11	19	26	28
Operating Time (h)	182	139	257	449	614	683
Charge Transfer	26351804	20125428	37056126	64682161	88562503	1.97E+08
C_Charge Transfer	26351804	46477232	83533359	1.48E+08	2.37E+08	4.34E+08
Number of Layer	2	2	2	2	2	2

A2: Bayesian Modelling Code in PyMC3

A2.1: Module import

In [ ]:
```
import pytensor.tensor as at
import arviz as az
import matplotlib.pyplot as plt
import pymc as pm

%config InlineBackend.figure_format="retina"
az.style.use("arviz-darkgrid")
```

A2.1: Bayesian Model using uninformative priors

```
with pm.Model(coords={"predictors":X.columns.values}) as RegressionMode2:
    #Specifying the Priors
    alpha=pm.Normal("alpha", mu=0, sigma=10)
    beta=pm.Normal("beta", mu=0, sigma=10, dims="predictors" )
    sigma=pm.HalfNormal("sigma", sigma=1)

    DegRate=pm.Normal("DegRate", alpha+ at.dot(X.values, beta), sigma=sigma, observed=y.values)

    #posterior Sampling
    trace=pm.sample(1000, tune=2000, random_seed=42, target_accept=0.99)
```

A2.2: Bayesian Model using regularised priors

In [ ]:
```
with pm.Model(coords={"predictors":X.columns.values}) as RegressionModel3:
    #Specifying the Priors
    sigma=pm.HalfNormal("sigma", sigma=25)

    tau=pm.HalfStudentT("tau", 2, D0/(D-D0)*sigma/np.sqrt(N))
    lam=pm.HalfStudentT("lam", 2, dims="predictors")
    c2=pm.InverseGamma("c2", 1, 0.1)
    z=pm.Normal("z", 0.0, 1.0, dims="predictors")


    beta=pm.Deterministic("beta", z*tau*at.sqrt(c2/(c2+tau**2*lam**2)), dims="predictors" )

    alpha=pm.Normal("alpha", mu=0, sigma=10) #Note regularization on the intercept


    DegRate=pm.Normal("DegRate", alpha+ at.dot(X.values, beta), sigma=sigma, observed=y.values)

    #posterior Sampling
    trace=pm.sample(1000, tune=2000, random_seed=42, target_accept=0.99)
```